”Origin of basaltic Subplinian eruption at Shishaldin volcano (Alaska): A vigorously degassing magma reservoir hosting small bubbles”

S Vergniolle

JGR Solid Earth

RESEARCH ARTICLE
10.1029/2023JB028161

Special Collection:
Advances in understanding volcanic processes

Origin of Basaltic Subplinian Eruption at Shishaldin Volcano (Alaska): A Vigorously Degassing Magma Reservoir Hosting Small Bubbles

S. Vergniolle[1]

[1]Université Paris Cité, Institut de Physique du Globe de Paris, CNRS, Paris, France

Key Points:

- The basaltic Subplinian eruption of Shishaldin is due to a very large underlying gas flux and tiny bubble diameter in the magma reservoir
- Four main basaltic regimes (weak and typical Strombolian, fire fountains, subplinian) can explained by foam behavior in magma reservoir
- The large gas flux in magma reservoir can be explained by the rise of tiny bubbles, agregated in bubble clusters, hence rising much faster

Supporting Information:

Supporting Information may be found in the online version of this article.

Correspondence to:

S. Vergniolle,
vergniolle@ipgp.fr

Citation:

Vergniolle, S. (2024). Origin of basaltic Subplinian eruption at Shishaldin volcano (Alaska): A vigorously degassing magma reservoir hosting small bubbles. *Journal of Geophysical Research: Solid Earth*, *129*, e2023JB028161. https://doi.org/10.1029/2023JB028161

Received 3 NOV 2023
Accepted 1 JUL 2024

Author Contribution:

Conceptualization: S. Vergniolle
Data curation: S. Vergniolle
Formal analysis: S. Vergniolle
Funding acquisition: S. Vergniolle
Investigation: S. Vergniolle
Methodology: S. Vergniolle
Resources: S. Vergniolle
Software: S. Vergniolle
Validation: S. Vergniolle
Visualization: S. Vergniolle

Abstract The 1999 basaltic eruption of Shishaldin volcano (Alaska) displayed a transition between Subplinian and Strombolian activity. Strombolian bubbles indicate the presence of a periodically unstable foam at the top of magma reservoir. In contrast, a long foam, whose rupture led to the eruptive column, was also able to collect in the conduit. Laboratory experiments show that long foams can be produced in a conduit by the spreading of a stable foam accumulated at the top of the reservoir. The existence of a Taylor bubble at the onset of the Subplinian phase, also reproduced by my laboratory experiments, suggests that the foam in the reservoir was just at the transition between stable and unstable. This constrains the bubble diameter prior to the Subplinian phase to be 0.034–0.038 mm when using the foam dimensionless analysis and the underlying gas flux (0.52–0.80 m^3/s). The increase in bubble diameter and potentially gas flux prior to the Strombolian activity, 0.81–1.4 m^3/s, is sufficient to explain the foam in transition to be unstable. The radius of the magma reservoir is small, 200–210 m, as expected. The bubble diameter is the smallest of those estimated for classical basaltic eruptions (Etna, Kīlauea, Erta 'Ale), while the gas flux is among the largest. A dilute suspension of small and isolated bubbles cannot explain the large gas flux at Shishaldin. This implies numerous bubbles with a gas volume fraction $\geq$0.63−2%, a regime for which the bubbles form bubble clusters. The diameter of these bubble clusters, 3.0–5.4 mm, is sufficient to explain large gas fluxes.

Plain Language Summary Basaltic eruptions, producing high eruptive columns, 16 km of ashes and volcanic gases, are rare and not yet well understood. The goal of this paper is to use the chronology of the 1999 Shishaldin eruption in Alaska, the estimates of expelled gas volumes obtained by previous studies of infrasound to understand this rare but dangerous eruptive regime. An analog volcano, no more than a few tens of centimeters, filled by viscous oils and small bubbles, was used to estimate key degassing parameters in the magma reservoir, that is, the diameter of the small bubbles and the gas flux at 3 km depth. The strength of this model is to be able to understand the four main basaltic eruptive patterns at the surface by a single set of parameters in the magma reservoir, the magma viscosity, the bubble diameter and the underlying gas flux.

1. Introduction

The role of bubbles has long been recognized as a critical parameter in the dynamics of eruptions (Navon & Lyakhovsky, 1998; Sparks, 1978; Sparks et al., 1994). Bubbles start forming at depth and grow during rise by gas diffusion and decompression. Because equations for bubble growth are complex even for a single bubble in an infinite liquid, various approximations have been discussed, for highly viscous magmas (Barclay et al., 1995), constant decompression rate (Lyakhovsky et al., 1996; Proussevitch & Sahagian, 1998; Toramaru, 1995) and constant ascent rate (Proussevitch & Sahagian, 1996). Another complexity comes from the interaction between neighboring bubbles, which may lead to bubble deformations favorable to bubble coalescence (Castro et al., 2012; Manga & Stone, 1995). A thin shell model has been proposed for bubbles packed in a foam (Barclay et al., 1995; Proussevitch et al., 1993). Bubbles at the surface are typically hundreds of microns to several millimeters in diameter for classical basaltic eruptions (Cashman & Mangan, 1994; Mangan & Cashman, 1996; Polacci et al., 2006, 2008, 2012) as well as for Subplinian activity (Stelling et al., 2002; Szramek et al., 2010) and for the paroxysmal activity at Stromboli (Bai et al., 2008). The gas volume fraction at fragmentation, one of the key parameters to understand fragmentation but not the sole one, is estimated to be ≈0.64, regardless of magma composition as soon as the magma viscosity exceeds ≈10^5 Pa.s (Gardner et al., 1996). Because bubbles in basaltic eruptions usually evolve after fragmentation due to their low viscosity, the vesicularity of basaltic scoria deposits does not record the fragmentation of basaltic Plinian eruptions (Gardner et al., 1996; Szramek et al., 2010).

Writing – original draft: S. Vergniolle
Writing – review & editing: S. Vergniolle

However, crystals can preserve the textures at fragmentation, at least at the rim (Szramek et al., 2010), in some of the basaltic Plinian eruptions, such as at Masaya (Nicaragua) and Llaima (Chile) (Arzilli et al., 2022; Bamber et al., 2022; Valdivia et al., 2022).

Parfitt and Wilson (1995) and Parfitt et al. (1995) suggested that the typical basaltic regimes resulted in a progressive bubble nucleation, growth and coalescence in the conduit while La Spina et al. (2021) parametrized the rise of a bubbly liquid in the conduit tuning their entry parameters to obtain either a Subplinian or a Strombolian activity.

Basaltic eruptions exhibit a cyclicity between quiescence and gas-rich periods such as Hawaiian high-level lava fountains or typical Strombolian explosions, unexplained by models discussed above (La Spina et al., 2021; Parfitt & Wilson, 1995; Parfitt et al., 1995). This cyclicity, results from the dynamics of a foam trapped at the top of the reservoir (Jaupart & Vergniolle, 1988, 1989), a model later validated by many independent measurements (e.g., Allard et al., 2005; Burton et al., 2007; Edmonds & Gerlach, 2007).

Basaltic eruptions displaying high-level eruptive columns are relatively rare, with only a handful of basaltic Plinian or Subplinian eruptions described in the literature, such as that at Masaya and Cerro Negro, Nicaragua, (Roggensack et al., 1997; Williams, 1983); Kīlauea ca. 1650 (Ferguson et al., 2016; Fiske et al., 1999, 2000), Fuego (Guatemala) (Lloyd et al., 2014; Rose et al., 2008), the An'ei eruption of Izu-Oshima (Japan) (Ikenaga et al., 2023) and Sunset crater (Arizona) (Alfano et al., 2018; Allison et al., 2021), Shishaldin (Alaska) (Stelling et al., 2002), Omok (Alaska) (Wong & Larsen, 2010), Llaima (Valdivia et al., 2022) and 1.8% of eruptions at Etna volcano (Coltelli et al., 1995, 2000). This list is made even shorter when phreatomagmatic eruptions (e.g., the initial and the final phases of the 1886 eruption of Tarawera, New Zealand; (Carey et al., 2007; Sable et al., 2009; Walker et al., 1984)) and silicic precursors to basaltic eruptions (Hekla, Iceland, (Thörarinsson & Sigvaldason, 1972)) are removed.

A number of mechanisms have been suggested to explain how fluid basaltic lava can generate an explosive high-level eruptive column. One means is through viscosity increases and transition to non-newtonian behaviour (Arzilli et al., 2022; Moitra et al., 2018), such as caused by microlite crystallization (Bamber et al., 2020; Houghton & Gonnermann, 2008; Moitra et al., 2018; Sable et al., 2009; Valdivia et al., 2022), vesiculation due to rapid magma decompression (Coltelli et al., 1998; Moretti et al., 2018), restriction of the effective radius of the conduit (Houghton et al., 2004; Sable et al., 2006), deep exsolution of CO_2 (Allison et al., 2021), multiple magma reservoirs and pathways (Ikenaga et al., 2023) or richness in volatiles (Roggensack et al., 1997). The role of the sole richness in volatiles is now questioned as no direct link was found between the intensity of the eruptions at Kīlauea and the concentration of pre-eruptive volatiles (Ferguson et al., 2016). Alternatively, a fast ascent rate was called for to explain the basaltic Plinian eruptions of Etna (122 BC) and Masaya (Fontana lapilli) (Namiki & Manga, 2006), due to a moderate richness in water, 3 wt% (Goepfert & Gardner, 2010). Similarly, the 1999 eruption at Shishaldin had been qualitatively interpreted as resulting from a fast ascent rate (Stelling et al., 2002), in agreement with its moderate richness in water, ≈2.5 wt% (Rasmussen et al., 2018). The magma ascent rate was also called for to explain both Subplinian and Strombolian activities, by fast and slow values, respectively (Larsen, 2016). At Cerro Negro, different decompression paths on a nearly identical magma have been thought to produce either an explosive (1992) or effusive (1995) basaltic eruption (Roggensack et al., 1997). A closed-system degassing within a new magma rising from depth, such that deduced for the 17 October 1974 episode at Fuego (Lloyd et al., 2014), is often called for to explain the basaltic (Sub)-plinian eruptions. However the degassing during the basaltic Subplinian and Plinian eruption of Shishaldin and Etna (122 BC eruption), respectively, had occurred as an open-system degassing (Moretti et al., 2018; Rasmussen et al., 2018; Stelling et al., 2002). Bombs have also a fluidal shape at Shishaldin (*P. Stelling*, pers.com.), showing that the magma fragmentation was ductile in the conduit whereas at the other extreme, bombs during the Oct 1974 episode at Fuego were sub-angular (Rose et al., 2008), hence indicative of a brittle fragmentation.

Basaltic (Sub)-plinian eruptions, which occurred with an open-system degassing, such as at Shishaldin (Rasmussen et al., 2018; Stelling et al., 2002) and Etna (Coltelli et al., 1998; Moretti et al., 2018), are still puzzling as the gas seems to be able to both move freely through the magma plumbing system and to be trapped in the conduit, such as to produce a high-level eruptive column, ≈16 km and ≈24–26 km in height, respectively (Coltelli et al., 1998; Nye et al., 2002). One option to explain the existence of Strombolian phases prior to a high-level eruptive column could be by turning the magma ascent rate from slow to fast during the eruption. However the occurrence of such a quasi-instantaneous change, such as required at Shishaldin (Caplan-Auerbach & McNutt, 2003; Figure 1), is very unlikely. A major recharge of magma, coming from a depth exceeding 20 km,

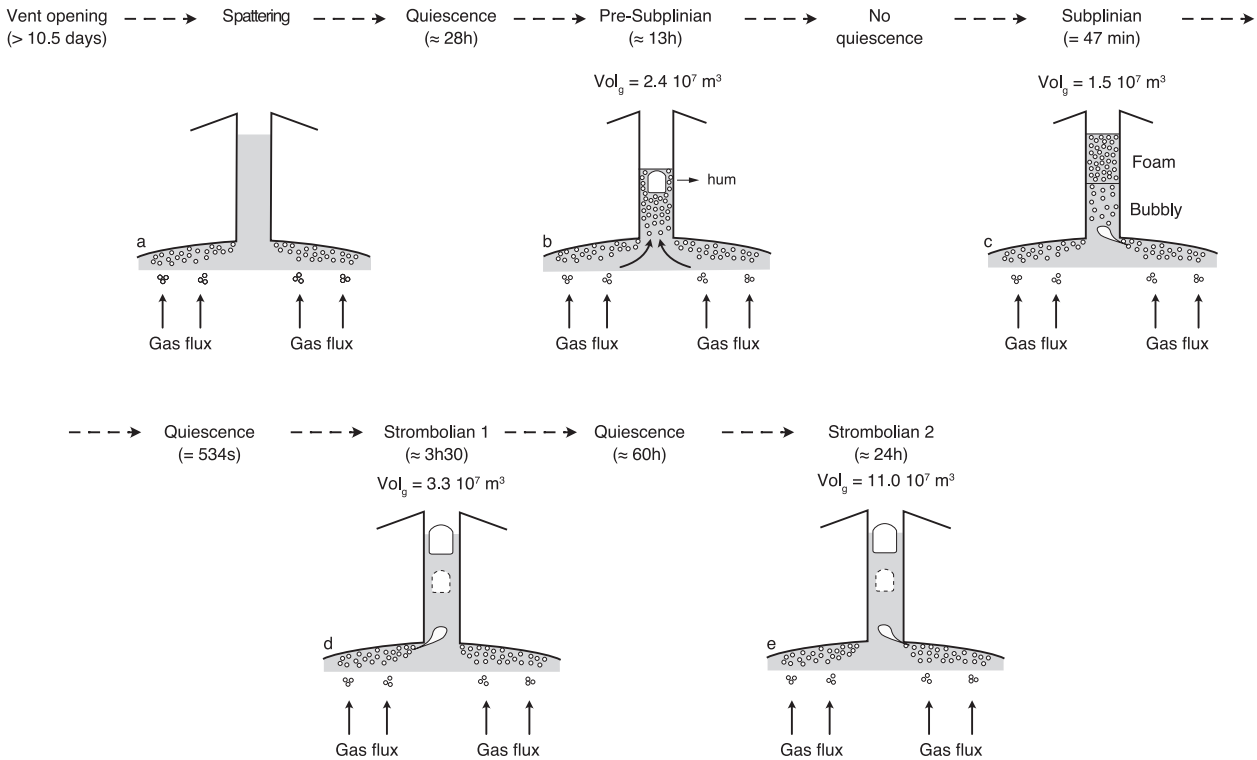

Figure 1. Interpretation of the chronology of the 1999 eruption of Shishaldin volcano with a simplified sketch of the Subplinian phase (see Vergniolle & Caplan-Auerbach, 2006 for details) with gas volumes at atmospheric pressure expelled during each phase of activity, Vol_g; (a) Unrecorded spattering phase of April 18 at 2:00 a.m., for a presumably start of the eruption on April 7 (Thompson et al., 2002); (b) Pre-Subplinian phase on April 19 with local coalescence events within a long foam, producing the "hum" events and the two thermals (Vergniolle & Caplan-Auerbach, 2004, 2006); (c) Generalized view of the Subplinian phase on April 19, initiated at 19:31, and producing one high-level eruptive column during ≈47 min while withdrawing more than half of the conduit (Vergniolle & Caplan-Auerbach, 2006); (d) first Strombolian phase starts just after the end of the Subplinian phase on April 19; (e) The second Strombolian phase on April 22–23 starts after 60 hr of quiescence; (f) Toward the end of the second Strombolian phase (on April 23 at 5:30), bubble overpressure at the vent is very large, up to ≈1.4 MPa, suggesting that the conduit is very rich in small gas bubbles (Vergniolle et al., 2004; Vergniolle and Caplan-Auerbach, 2006).

occurred 50 days before the first observation of the eruption, while a minor mixing event had occurred 11 months before (Rasmussen et al., 2018), suggesting no obvious change in the magma ascent rate.

Infrasonic measurements during the 1999 eruption at Shishaldin had provided invaluable estimates of the gas volumes produced at the vent during the pre-Subplinian phase (Vergniolle & Caplan-Auerbach, 2004), the Subplinian phase (Vergniolle & Caplan-Auerbach, 2006) and the two Strombolian phases (Vergniolle et al., 2004). Investigating these eruptive transitions in the light of the estimated degassing may be the key to determining what causes a relatively placid eruption to exhibit more violent behavior. We have proposed that the basaltic Subplinian eruptive column results from the disruption of a long foam, ≈2.0 km, accumulated in the conduit (Vergniolle & Caplan-Auerbach, 2006). The novelty of my paper is primarly to suggest a mechanism for building-up a long foam in the conduit not based on a sudden decompression, as nonexistent at Shishaldin.

Here, I suggest that the foam builds in the conduit because the foam trapped at the top of the reservoir is stable and spreads radially, focusing a large gas flux accumulated onto a relatively large surface into a small conduit. I reproduce this condition by laboratory experiments in order to mimic the conditions prevailing at the initiation of the Subplinian phase and explore the consequences on eruption dynamics. I then determine gas volume fraction, bubble diameter and gas flux in the reservoir independently. The aim of this paper is to add a new basaltic regime, the rare basaltic high-level eruptive column, into the single framework already developped for high-level lava fountains and Strombolian activity (Jaupart & Vergniolle, 1988, 1989; Vergniolle & Jaupart, 1990) and for the weak Strombolian activity at Erta 'Ale (Vergniolle & Bouche, 2016). Here I show that any basaltic activity only results from the values of three parameters in the reservoir, namely gas flux, magma viscosity and bubble diameter. I further propose that the bubble population in the magma reservoir results from different magma ascent

rate at four volcanoes, very large for Shishaldin, large for the Kilauea Iki eruption at Kīlauea, intermediate at Etna and small at Erta 'Ale.

2. Description of Eruptive Activity

Shishaldin volcano is located above the North Pacific subduction zone. The regional setting, geologic history and instrumentation in place at Shishaldin are described in Beget et al. (2003), Stelling et al. (2002), Thompson et al. (2002) and Caplan-Auerbach and McNutt (2003).

For the purposes of this paper, I reiterate that Shishaldin eruptions prior to 1999 were often brief with basalts to basaltic-andesite magmas (Nye et al., 2002). However Shishaldin went into a fairly prolonged series of Strombolian explosions since 1999 (Cusano et al., 2015; Fee et al., 2021; Petersen et al., 2006; Petersen & McNutt, 2007) and produced small, ≈200 m, discrete steam plumes exiting at the summit crater (Petersen & McNutt, 2007). The omni-present steam plume and steam puffs together with repetitive LP events, coupled in short-period and long-period bands, may be related to degassing (Caplan-Auerbach & Petersen, 2005).

Eruptive activity at Shishaldin is often associated with small steam and ash plumes at the summit. One hundred tephra layers have been deposited by plume eruptions over the last 9000 years, however only 11 of them are as widespread and voluminous as the 1999 eruption (Beget et al., 1998; Stelling et al., 2002). Strombolian activity is also frequent either at the summit or on the flanks, as marked by the 55 basaltic cinder cones on the volcano flanks (Nye et al., 2002).

The exact start of the eruption is unclear due to poor weather, but the sudden increase of the tremor level on 7 April 1999 suggests that the eruption had started on this day at ≈18:00 (all times in the paper are UTC) (Thompson et al., 2002). The 1999 eruption was first confirmed on April 18 at 02:00 when researchers from Alaska Volcano Observatory (AVO) observed spattering within the summit crater (Nye et al., 2002). The eruption, as detected by infrasonic and seismic sensors, built up in strength, during the pre-Subplinian phase (Caplan-Auerbach & McNutt, 2003; Thompson et al., 2002). This phase was marked by a close series of weakly overpressurized large bubbles, called “hum” events, interrupted in the middle by the disruption of two small eruptive columns, called thermal phases (Vergniolle & Caplan-Auerbach, 2004, 2006) (Figure 1). This “humming signal” is interpreted by a close series of bursting of large bubbles resulting from local coalescence within a long foam building up in the conduit (Figure 1) (Vergniolle & Caplan-Auerbach, 2004, 2006). The humming signal stopped immediately before a Subplinian phase brought an ash plume to heights greater than 16 km (Nye et al., 2002). The initiation of this high-level eruptive column is marked by the bursting of a very overpressurized quasi-cylindrical Taylor bubble, called the trigger bubble (Vergniolle & Caplan-Auerbach, 2006). Shortly after the Subplinian phase, a sequence of signals interpreted as Strombolian bubble bursts were detected on infrasonic records (Figure 1) (Vergniolle et al., 2004). Two episodes of Strombolian activity occurred, on April 19–20 and again on April 22–23, both quantified in terms of bubble radius, length and overpressure (Vergniolle et al., 2004). The time at which the eruption ended is not well constrained due to a lack of visual observations and infrasonic data. The large ash plume of May 25–26 is believed to be the final major episode of the 1999 eruption (Nye et al., 2002). However, I consider that the eruption has mainly stopped at the end of the second Strombolian phase since the late ash plumes occurred very infrequently.

3. Independent Constraints on Magma at Depth

In this section, I discuss the constraints existing on the parameters, later used in my model.

3.1. Calculation of Melt Viscosity From Melt Inclusions

The location of Shishaldin at the transition between the oceanic and continental subduction domains leads to a magma of tholeitic composition during the 1999 eruption but richer in water, with a maximum of ≈2.5 wt% (Rasmussen et al., 2018), than that of Kīlauea, ≈0.8 wt% (Edmonds et al., 2013; Ferguson et al., 2016).

More than fifty melt inclusions were analyzed to obtain magma composition, volatile content, temperature and depth of storage, when assuming chemical equilibrium (Figure 2) (Rasmussen et al., 2018, https://doi.org/10.1016/j.epsl.2018.01.001). The water content in the melt inclusions, corrected for the fast diffusion of water after the closing-up of the melt inclusion using a relationships between sulfur and water, leads to an estimate for the depth of entrapment for each melt inclusion (Rasmussen et al., 2018). The depth of storage, that is, the depth at which melt

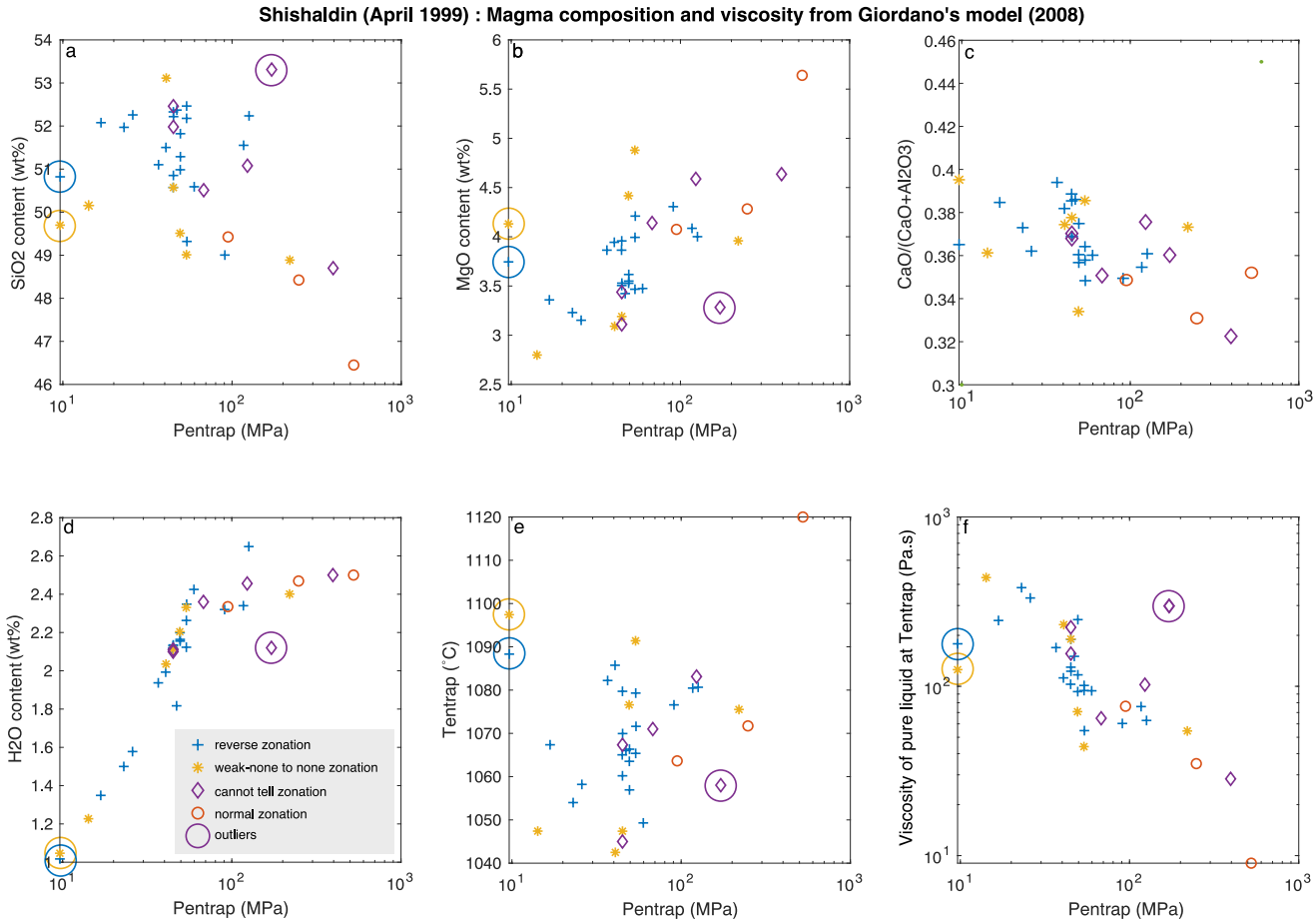

Figure 2. Results on magma composition from melt inclusions as a function of the pressure of entrapment, P_{entrap}, that is, the initial pressure at which the melt inclusion forms (Rasmussen et al., 2018) (see text for details) with (a) SiO_2 content (wt%), (b) MgO content (wt%), (c) the ratio $CaO/(CaO + Al_2O_3)$, (d) H_2O content (wt%), (e) Temperature of entrapment, T_{entrap} (°C) and (f) the melt viscosity (Pa.s) using Giordano et al.' s model, (2008a, 2008b) and assuming no crystals in the melt. The magma viscosity is multiplied by a factor 2.5 (Mader et al., 2013) when adding 29% of phenocrysts, the maximum possible (Stelling et al., 2002). The increase in SiO_2 content and in the ratio $CaO/(CaO + Al_2O_3)$, the decrease in MgO and in H_2O contents at a pressure of 60 MPa show that the crystallisation, already started in the reservoir (Stelling et al., 2002), is significantly enhanced at this depth and above. The blue crosses, orange stars, purple diamonds and red circles represent the type of zonation in the host crystal, reverse, weak-none to none, undetermined and normal, respectively (Rasmussen et al., 2018) (see text for details). The purple circles are values which may be outliers. The magma viscosity at 60 MPa, assumed to be the depth of the reservoir (Rasmussen et al., 2018) is ≈60 Pa.s and stays around this value up to ≈120 MPa before decreasing at larger depths.

inclusions had stayed for duration ≥ hours-day, varies between the surface and a depth of 3 km, while the depth of entrapment varies between 2 and 20 km (Rasmussen et al., 2018). The melt viscosity, defined as being that of a magma without crystal (μ_{liq}; Table 1), was estimated for each melt inclusion from the melt composition, water content and temperature, all restored at the depth of entrapment (Rasmussen et al., 2018), using the Giordano et al. (2008a, 2008b)'s model for the viscosity, well adapted for basaltic melts with dissolved water (Figure 2, Vergniolle, 2024a, 2024b). Four groups of melt inclusions have been distinguished, as a function of the host crystal zonation, which could be reverse, normal, weak to absent or unknown (Rasmussen et al., 2018). The reverse zonation results from an interaction between a resident magma and a new magma, likely to have occurred in the conduit, while the normal zonation indicates a perfect mixing stage, likely to have occurred in the reservoir and at depth.

The evolution of the water content with the depth of entrapment (Figure 2) is fairly smooth, reaching an assymptotic value of 2.5 wt% at ≈60 MPa, hence a depth of 3 km. The melt viscosity clearly shows the largest value close to the surface, a well marked and steep descending gradient around 40–60 MPa, a plateau between 60 and 120 MPa, which could represent the thickness of the shallow magma reservoir, and a slow descent toward the largest pressures (Figure 2). The steep gradient in magma viscosity at pressures of 40–60 MPa, also clear on the

Table 1
Lists of Symbols Used Throughout the Text

Variable	Definition	Equations
C_{geom}	Geometrical coefficient	5
d_{clust}	Diameter of bubble cluster (m)	10, 11
d_{foam}	Diameter of bubble in foam (m)	1
d_{res}	Diameter of bubble in reservoir (m)	2,7, 9
d_{surf}	Diameter of bubble at surface (m)	6
g	Acceleration of gravity (m.s^{-2})	1, 2,6, 7, 9, 10
h_{crit}	Critical height of foam (m)	4
h_{max}	Maximum height of foam (m)	4
k_{koz}	Kozeny constant	1
N_1	Dimensionless foam height	2
P_{atm}	Pressure at atmosphere (Pa)	6
P_{resSub}	Pressure in reservoir prior Subplinian (Pa)	6
Q_{clust}	Gas flux of bubble cluster in reservoir (m^3.s^{-1})	11
Q_{res}	Gas flux in reservoir (m^3.s^{-1})	2, 9
R_{cond}	Radius of conduit (m)	5
R_{eclust}	Reynolds number of bubble cluster	12
R_{res}	Radius of reservoir (m)	5
S_{res}	Surface of reservoir (m^2)	7, 9, 11
U_{koz}	Drainage velocity in foam (m.s^{-1})	1
U_{clust}	Velocity of bubble cluster (m.s^{-1})	1
V_{foam}	Volume of foam (m^3)	7, 8
V_{gas}	Volume of gas in foam (m^3)	8
α	Gas volume fraction in reservoir	9
α_{clust}	Gas volume fraction of bubble cluster	11
ϵ	Gas volume fraction in foam	1
ϵ_{clust}	Gas volume fraction within bubble cluster	in text prior to Equation 10
ϵ_{res}	Gas volume fraction in foam trapped in reservoir	3
μ_{clust}	Viscosity of bubble cluster (Pa.s)	10
μ_{foam}	Viscosity of foam (Pa.s)	2
μ_{liq}	Viscosity of liquid (Pa.s)	1, 9, 10, 12
ρ_{clust}	Density of bubble cluster (kg.m^{-3})	10
ρ_{gas}	Density of gas (kg.m^{-3})	9
ρ_{liq}	Density of liquid (kg.m^{-3})	1, 9, 10, 12
σ	Surface tension (kg.s^{-2})	2

Note. The label "Equations" refers the the number of the equation in which the symbol appears. The indexes "foam," "res," "clust" refer to the foam, the reservoir, the bubble cluster.

silica, magnesium content and the ratio CaO/(CaO + Al_2O_3) (Figure 2). This suggests that the crystallization had taking place at these locations, the deepest being interpreted to be the base of the conduit. The magma viscosity, when including the 29 vol% of total crystallinity content (including crypto-crystallinity, microliths and phenocrysts) observed in the samples (Stelling et al., 2002), whose matrix glass composition and bulk-rock composition are fairly similar (Rasmussen et al., 2018), is increased by a factor 2.5 when ignoring the unknown crystal shape (Figure 5 in Mader et al., 2013). However it is not possible at this stage to know at which pressure the crystals are formed in amounts significantly large to be able to change the magma viscosity. This prevents us to obtain a more detailed profile for the magma viscosity in the conduit.

3.2. A Magma Reservoir Rich in Volatiles

One surprising feature of the 1999 eruption at Shishaldin is its lack of observed deformations of the volcanic edifice prior and around the time of the eruption (Lu et al., 2003, 2007; Moran et al., 2006). This could be related to either the long delays between the InSAR images or the shape of the existing magma reservoir, with a small surface area and perhaps a cylindrical shape. Chemical data from melt inclusions suggest that the magma stays in the shallow magma reservoir sufficiently long a time to be able to grow olivine phenocrysts (Stelling et al., 2002). Furthermore the storage depth of all the melt inclusions, between 0 and 3 km, had led Rasmussen et al. (2018) to explain the lack of deformation by the existence of a small and/or cylindrical reservoir, whose top is located at a pressure of 60 MPa, hence at a depth of ≈3 km when assuming a magma density of 2,200 kg.m^{-3}. Another indirect constraint on the magma reservoir at Shishaldin comes from infrasonic measurements of the trigger bubble, thought to have induced the Subplinian phase (Vergniolle & Caplan-Auerbach, 2004, 2006). The gradual increase, observed in the low frequency range of infrasonic pressure before the trigger bubble arrives at the surface, has been associated with the rise of this Taylor bubble from the depth of the magma reservoir (Vergniolle & Caplan-Auerbach, 2006). This suggests that the reservoir is located at ≈3.9 km (Vergniolle & Caplan-Auerbach, 2006), which corresponds to a pressure of 74 MPa when assuming a foam of ≈2.0 km long in the conduit (Vergniolle & Caplan-Auerbach, 2006) and a magma density of 2,700 kg.m^{-3}, just slightly above the value of 2,600 kg.m^{-3} used by Stelling et al. (2002). This is in very good agreement with the estimates from melt inclusions, ≈60 MPa (Rasmussen et al., 2018). In the rest of the paper, I assume that the shallow magma reservoir is located at 3 km below the summit (Table 2).

The existence of a shallow magma reservoir and the richness in volatiles of the magma, such as the gas is already exsolved at its depth, are the two key ingredients on which the foam model is based (Jaupart & Vergniolle, 1988, 1989; Vergniolle & Jaupart, 1990). These laboratory experiments have shown that the foam stability is well described with a fairly minor constriction between the radius of the reservoir and that of the conduit, a factor 6 being typically used but even a factor 3 being sufficient (Jaupart & Vergniolle, 1989). I shall now discuss the constraints brought by the tremor on the estimates of the gas flux in the magma reservoir before going into the applicability of the foam model to the eruptive patterns at Shishaldin.

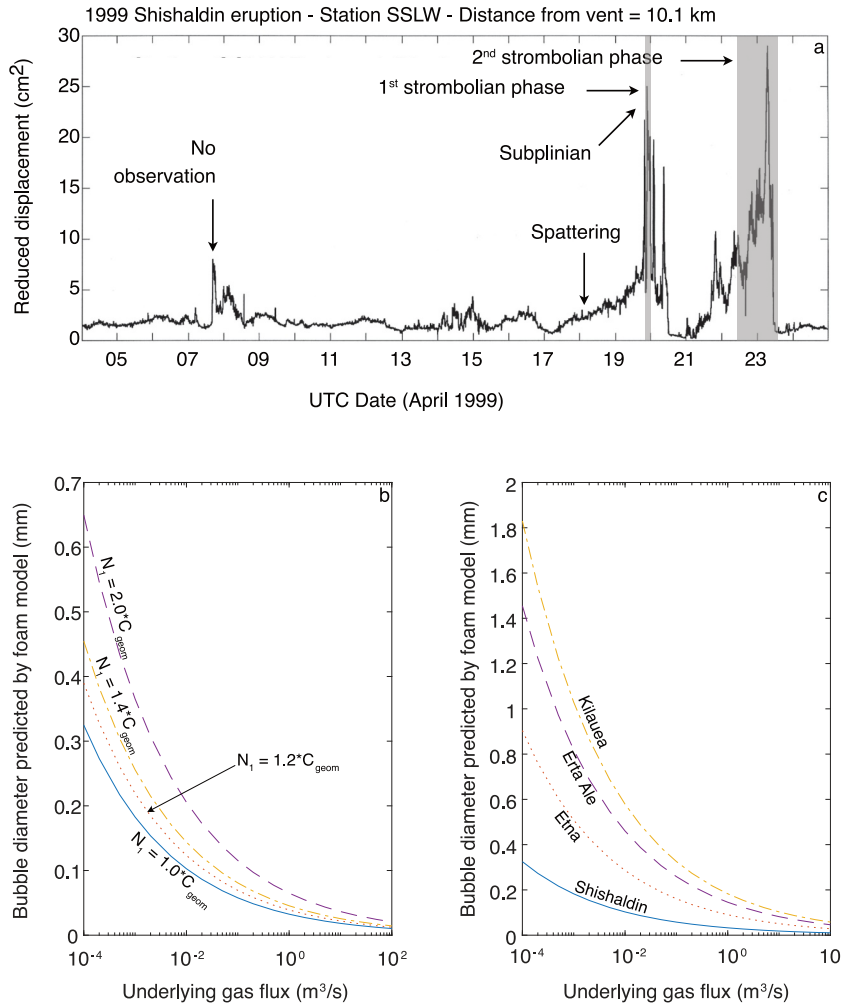

Figure 3. (a) Reduced displacement of the tremor (cm^2) (Thompson et al., 2002) as a function of time in days. It is calculated each 10 min at the distance of 10.1 km (SSLW) from the likely start of the eruption on 7 April 1999 to the end of the second Strombolian phase, which mostly marks the end of the eruption (adapted from Figure 3 in Thompson et al., 2002). Data are filtered above 0.8 Hz to remove the oceanic noise. The tremor increases very regularly (around the April 17 at ≈0:00) before the Subplinian phase and before the second Strombolian phase (around the April 20 at ≈12:00). The first Strombolian phase occurs very quickly after the Subplinian phase and lasted 3 hr and a half (Figure 1). The regular increase prior to the second Strombolian phase suggests that it initiated at depth a few days before its surface expression. The tremor increase on April 17 and April 20 suggests to use a timescale of 63 hr 31 min and 36 hr for the foam accumulation at the top of the reservoir before the Subplinian phase and the second Strombolian phase, respectively. These two timescales become 41 hr 31 min and 60 hr, respectively, when using the surface activity as a clock marking the start of the foam accumulation in the reservoir; (b) Role of the dimensionless foam height, N_1, onto the bubble diameter predicted by the foam model (Equation 2); (c) Bubble diameter predicted by the foam model (Equation 2), assuming that the geometrical coefficient, $C_{geom} = 0.64$ (Equation 5), as for Shishaldin and Etna, and for the conditions of magma viscosity and surface tension at Shishaldin $\mu_{liq} = 60$ Pa.s (Figure 2); $\sigma = 0.1$ kg.s^{-2}), Etna ($\mu_{liq} = 1$ Pa.s (Métrich et al., 2001); $\sigma = 0.1$ kg.s^{-2}), Erta 'Ale ($\mu_{liq} = 25$ Pa.s (Vergniolle and Métrich et al., 2022); $\sigma = 0.36$ kg.s^{-2}) and Kīlauea ($\mu_{liq} = 10$ Pa.s (Vergniolle, 2008); $\sigma = 0.36$ kg.s^{-2}).

3.3. Tremor Records

Several models have been proposed to explain the volcanic tremor, among which the degassing had been suggested to be a likely source at basaltic volcanoes (e.g., Caplan-Auerbach & Petersen, 2005; Ripepe & Gordeev, 1999; Ripepe et al., 2001) (see Supporting Information S1).

At Shishaldin, the tremor (Thompson et al., 2002) was recorded on short period seismometers at distances up to 17 km from the vent. The very sharp increase in tremor intensity on April 7 at 18:00 probably marks the opening of the vent (Thompson et al., 2002). The Subplinian phase (April 19, 19:31) and the peak in overpressure during

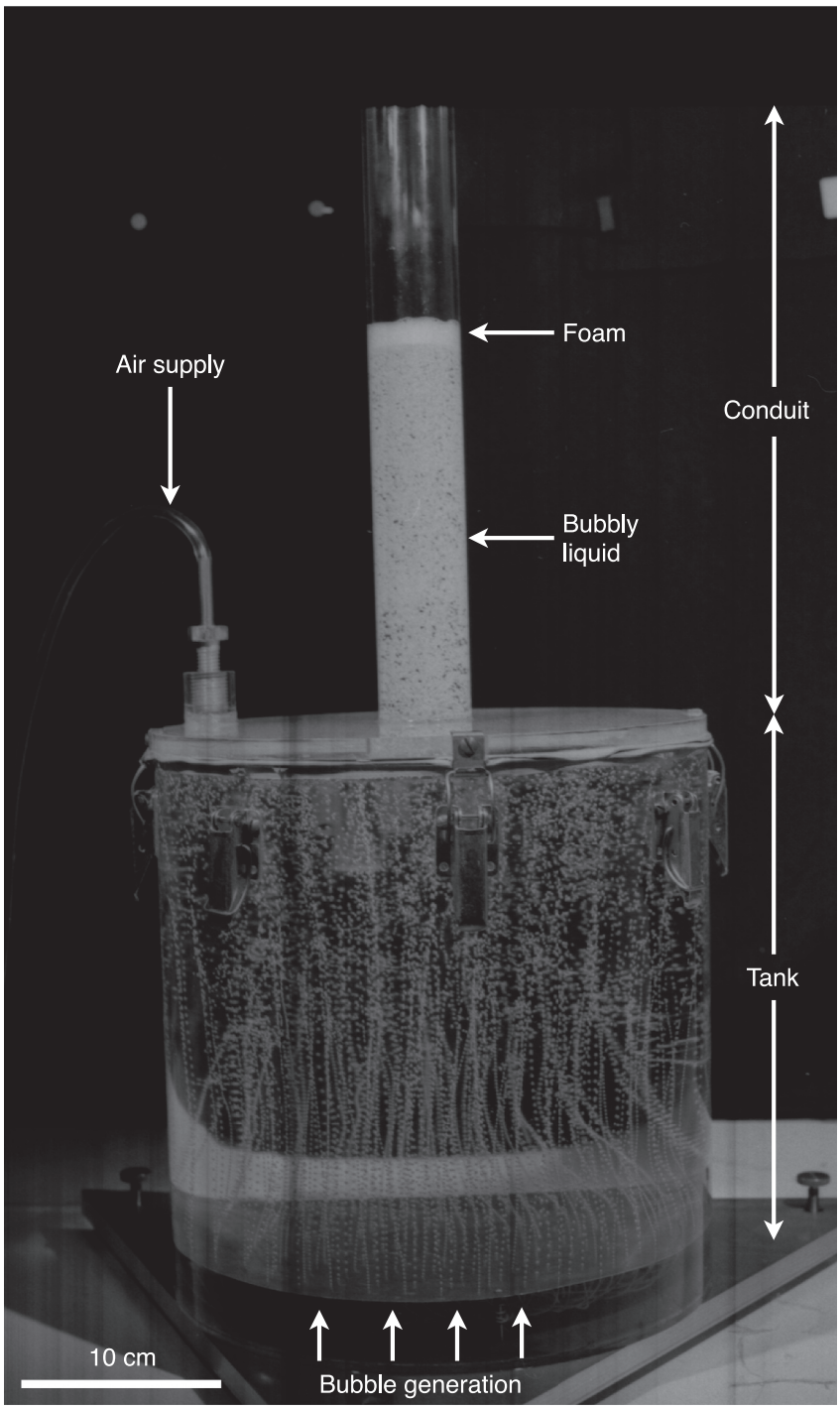

Figure 4. Laboratory experiments in an analog volcano with tank diameter and conduit diameter of 0.044 and 0.28 m, respectively. The apparatus was filled with silicone oils (Rhodorsil 47V10) with a viscosity of 0.0093 Pa.s. The gas is supplied by a N_2 bottle to prevent gas diffusion into the existing bubbles at a gas flux equal to $\approx 6.7 \times 10^{-6}$ m^3/s. The small bubbles were produced at the base of the reservoir by a set of 185 identical capillaries, with an inner diameter of 0.38 mm, regularly spaced. The specificity of the apparatus is to be able to produce a population of quasi-identical small bubbles, 1.5 mm in diameter, within an error of $\leq 10\%$. Two foams can be seen, one at the top of the reservoir (bottom part of the photograph) and one in the conduit (white color).

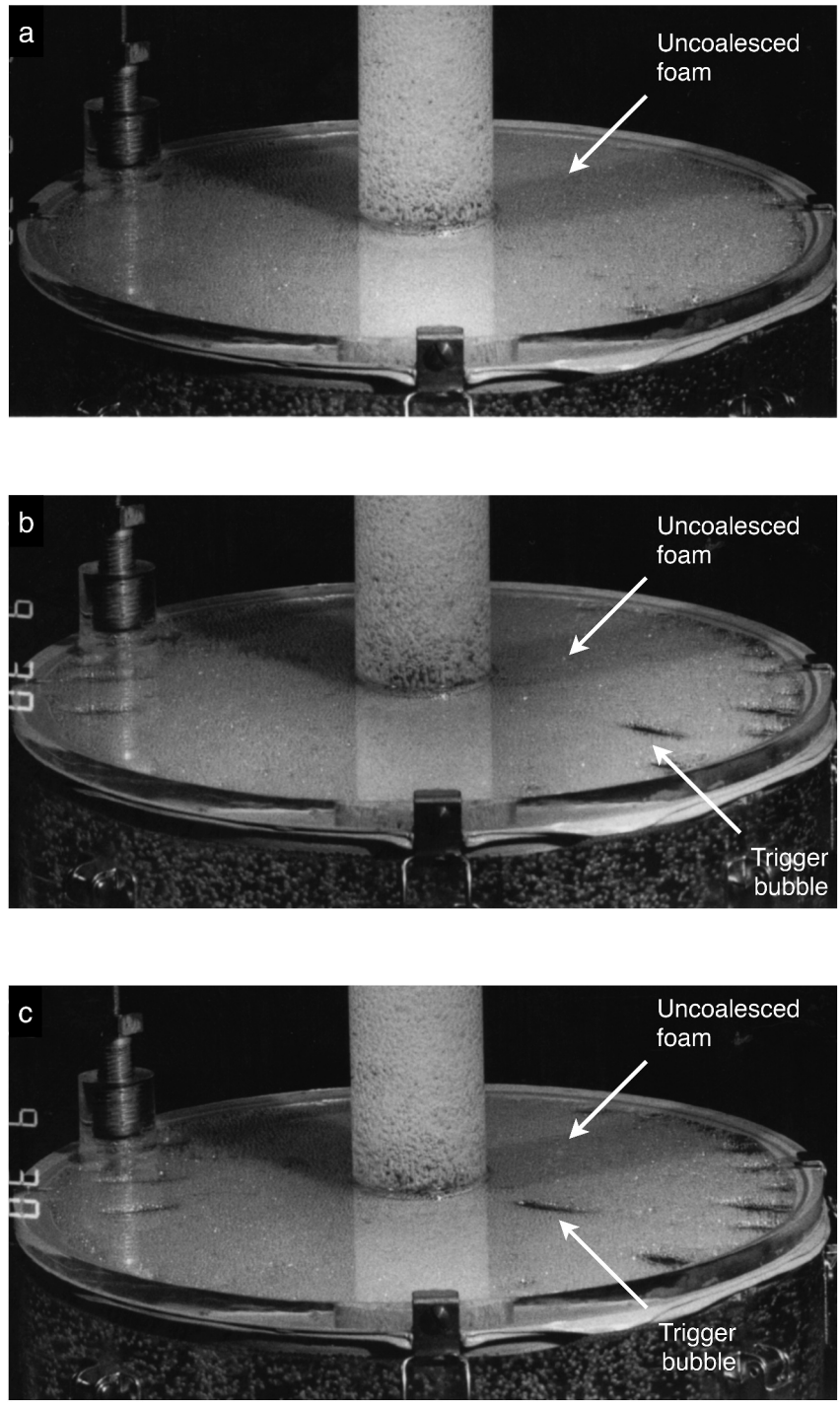

Figure 5. Enlargement of the top of the reservoir for each photo presented in Figure 6 with an exact equivalence of indexes between figures, showing the building-up of a foam (white color) produced under a gas flux of $\approx 1.7 \times 10^{-5}$ m^3/s with silicone oil 47V10 (see details in Figure 4). (a) stable foam (white color) with very little tiny gray patches (locally coalesced foam) potentially corresponding to foam ripening; (b) local foam coalescence producing gas pockets (dark color) at the outer edges of the reservoir, resulting from the thickening of the foam over its critical thickness, hence starting the massive foam coalescence. The trigger bubble corresponds to the gas pocket closest to the conduit and seen migrating toward it, as a consequence of the foam spreading; (c) trigger bubble, approaching the conduit while new gas pockets resulting from the massive foam coalescence are produced at the outer edges of the reservoir.

Table 2
Various Estimates of the Degassing Reservoir, Bubble Diameter, D_{res}, Radius of Magma Reservoir, R_{res}, Diameter of Bubble Clusters, D_{clust} for Two Gas Volume Fractions, α_{clust} Equal to 2% and 0.63%, Reynolds Number of the Bubble Clusters, R_e, for Two Reference Foams Accumulated in the Reservoir With a Gas Volume Fraction ϵ_{res} of 0.6 and 0.3

Reservoir at depth ($z_{res} \approx 3$ km; $\mu \approx 60$ Pa.s) | ϵ_{res} =	0.6	0.3	0.6	0.3
Density, ρ_{liq} (kg.m^{-3})	2700	2700	2700	2700
Viscosity, μ_{liq} (Pa.s)	60	60	60	60
Surface tension, σ (kg.s^{-2})	0.1	0.1	0.1	0.1
Conduit radius, R_{cond} (m)	6	6	6	6
Prior to Subplinian phase				
Measurements	Tremor	Tremor	Surface	Surface
Repose time (hr)	63.5	63.5	41.5	41.5
Gas flux before Subplinian (m^3/s)	0.52	0.52	0.8	0.8
Bubble diameter d_{res} (mm)	0.038	0.077	0.034	0.069
Radius of magma reservoir, R_{res} (m)	210	300	200	280
Gas volume fraction for clusters $\alpha_{clust} = 2\%$				
Diameter of bubble cluster d_{clust} (mm)	3.5	2.5	4.6	3.2
Reynolds number R_e ($\times 10^{-5}$)	2.9	1.0	6.6	2.3
Gas volume fraction for clusters $\alpha_{clust} = 0.63\%$				
Diameter of bubble cluster d_{clust} (mm)	5.4	4.4	8.2	5.8
Reynolds number R_e ($\times 10^{-5}$)	17	5.9	37	13
Bubble diameter at surface d_{surf} (mm)	0.33	0.65	0.29	0.58
Prior to 2nd Strombolian phase				
Measurements	Tremor	Tremor	Surface	Surface
Repose time (hr)	36	36	60	60
Gas flux before Strombolian (m^3/s)	1.4	1.4	0.81	0.81
Foam model: $N_1/C_{geom} = 1.2$ and $C_{geom} = 0.64$				
Bubble diameter d_{res} (mm)	0.036	0.072	0.041	0.082
Gas volume fraction for clusters $\alpha_{clust} = 2\%$				
Diameter of bubble cluster d_{clust} (mm)	5.7	4.0	4.6	3.2
Reynolds number R_e ($\times 10^{-5}$)	12	4.0	6.6	2.3
Gas volume fraction for clusters $\alpha_{clust} = 0.63\%$				
Diameter of bubble cluster d_{clust} (mm)	10	7.1	8.2	5.8
Reynolds number R_e ($\times 10^{-5}$)	70	24	37	13
Bubble diameter at surface d_{surf} (mm)	0.30	0.61	0.34	0.69

Note. Magma density, surface tension and conduit radius are given by Williams and McBirney (1979), Khitarov et al. (1979) and Vergniolle et al. (2004), respectively. The repose time used to calculate the gas flux is either based on the tremor intensity (labeled "Tremor," Figure 3a) or surface activity, (labeled "Surface," Figure 1). Bubble diameter at the surface, d_{surf}, is calculated using the ideal gas law (Equation 6) and its value at the depth of the magma reservoir.

the second Strombolian phase (April 23, 8:00), are evident at times marked 19 and 23 on Figure 3a. Tremor increase begins 2 days and a half before the start of the pre-Subplinian phase and increases regularly until the start of the Subplinian phase between times 17 and 19 on Figure 3a. A similar phenomenon occurs before the second Strombolian phase, although with a faster increase and more variation between times 22 and 23 on Figure 3a.

The regular tremor increase prior to surface activity (Figure 3a) suggests that the Subplinian and Strombolian phases initiate at depth a few days before their surface expression. In contrast, the first Strombolian phase, although starting at a high level, appears as an erratic drop in the tremor intensity, suggesting that most of the foam trapped in the reservoir is quickly escaping due to the decompression induced by the Subplinian eruptive column.

This is in agreement with both the short delay between the end of the Subplinian phase and the start of the first Strombolian phase, ≈534 s (Figure 1) and the marked difference in bubble length and gas overpressure displayed by the two Strombolian phases, with ≈82 m and ≈0.083 MPa and ≈24 m and ≈0.15 MPa for the first and the second Strombolian phase, respectively (Vergniolle et al., 2004). In this framework, the similarity in gas volumes, at atmospheric pressure, between that expelled by the trigger bubble, $\approx 1.3 \times 10^4$ m^3, and that by a typical Strombolian bubble during the first phase, $\approx 1.2 \times 10^4$ m^3, which is 6 times larger than that during the second Strombolian phase, $\approx 1.9 \times 10^3$ m^3, (Vergniolle et al., 2004), suggests to consider the trigger bubble as directly resulting from a coalescence event within the foam accumulated in the reservoir.

Note that there is another pulse in the tremor, which corresponds to the few weakly overpressurized bubbles of April 20 (Caplan-Auerbach & McNutt, 2003; Thompson et al., 2002; Vergniolle et al., 2004), whose gas volume, potentially very small, has not been considered.

3.4. Gas Flux in the Reservoir

One ingredient necessary to predict the behavior in the degassing reservoir from a model based on the foam dynamics is the underlying gas flux at the top of the magma reservoir (Jaupart & Vergniolle, 1989; Vergniolle & Jaupart, 1990). This gas flux depends on the gas volume at depth and the time taken by the foam to accumulate before being unstable. The gas volume at the depth of the reservoir, assumed to be 60 MPa (Rasmussen et al., 2018), can be estimated at this depth from the gas volume expelled at the surface assuming an ideal gas. The gas volume at the surface and the duration for the four major phases of the Shishaldin eruption have been deduced from infrasonic measurements (Figure 1). I postpone the discussion on the potential errors brought to light by more recent studies on jet noise (Fee et al., 2017; Ichihara, 2016; Matoza et al., 2013) and radiation patterns (Jolly et al., 2017; Kim et al., 2012; Matoza et al., 2009; Tam et al., 2008) to Appendix A and the section "sensitivity analysis" in the Supporting Information S1.

The characteristic timescale for foam accumulation in the reservoir prior to the Subplinian or the second Strombolian phase could be based on surface activity (Figure 1) or on the temporal evolution of the tremor amplitudes (Figure 3a). I favor the latter (details can be found in the Supporting Information S1), and present the results for both timescales in Table 2. I use the gas volumes expelled during the pre-Subplinian, Subplinian and first Strombolian phases to calculate the gas flux in the reservoir prior to the Subplinian phase (Equation 3 in (Vergniolle & Gaudemer, 2012); Supporting Information S1) and that expelled during the second Strombolian phase for that prior to this phase (Table 2).

In these conditions, the gas flux in the magma reservoir is markedly larger after than before the Subplinian phase if based on the tremor amplitudes, with ≈0.52 m^3/s and ≈1.4 m^3/s for the Subplinian and Strombolian phases, respectively (Table 2). However, the gas flux is similar if based on surface activity, with ≈0.80 m^3/s and ≈0.81 m^3/s for the Subplinian and Strombolian phases, respectively (Table 2). I use the gas flux estimated before the Subplinian phase to interpret the chronology of the eruption.

4. Formation of a Long Foam in a Volcanic Conduit

A striking result of the 1999 eruption of Shishaldin is the existence of a Subplinian phase, corresponding to a sustained dispersed gas flow made of a gas jet carrying small ejecta. Such a dispersed gas flow could be easily obtained by the sudden rupture of a long foam accumulated in the conduit, in a process possibly similar to fragmentation, which can be ductile or fragile. The large amount of gas produced during the Subplinian phase, 1.5×10^7 m^3 (Vergniolle & Caplan-Auerbach, 2006), after being organized within a foam and compressed according to its local depth, corresponds to a very long foam, ≈2.0 km, accumulated in the conduit prior to the Subplinian phase (Vergniolle & Caplan-Auerbach, 2006). Note that the lack of initial decompression at the initiation of the Subplinian phase, as unobserved on seismic and infrasonic records (Caplan-Auerbach & McNutt, 2003; Thompson et al., 2002; Vergniolle & Caplan-Auerbach, 2006), discards a mechanism of foam build-up based on a sudden bubble exsolution and growth in the conduit upon decompression, as envisioned for explosive volcanoes. This also discards a fragile fragmentation at the initiation of the Subplinian phase.

The three key features of the Subplinian phase consists (1) in the building up of a long foam in the conduit, (2) its sudden rupture, combined with (3) the quasi-simultaneous breaking of a single large overpressurized bubble at the vent, only 28 s after the start of the high-level eruptive column (Vergniolle & Caplan-Auerbach, 2004, 2006).

Because the magma reservoir at Shishaldin is rich in gas, with a total water content of 2.2–2.6 wt% (Rasmussen et al., 2018), I suggest that a foam exists at the top of the reservoir, whose dynamics is responsible for the formation of basaltic high-level eruptive columns.

In this paper, the laboratory experiments could only be designed to reproduce the formation of a long foam in the conduit (1) and the formation at depth of a single Taylor bubble, that is, the trigger bubble, prior to its bursting at the surface, as observed on infrasonic records (3) (Vergniolle & Caplan-Auerbach, 2004, 2006). These two features were not so straightforward to obtain as isolated items and even less when combined. The detailed mechanism by which a long foam can suddenly be destroyed (2) is the subject of another paper involving different laboratory experiments.

4.1. Theory on Foam Drainage and Stability

In this section, I present firstly a theory for the foam drainage in the conduit and secondly a theory on the stability of a foam accumulated at the top of the magma reservoir. I then discuss the laboratory experiments used to mimic the eruptive pattern during the 1999 Shishaldin eruption. Lastly, I apply these theories to the case of Shishaldin.

4.1.1. Theory on Foam Drainage

A stationary foam in the conduit can drain and have its interstitial films shrinking until reaching a critical thickness. At this stage, the drained part of the foam can be easily destroyed, thereby expelling its gas into the atmosphere and reducing the foam height. The gravity is the main driving mechanism of foam drainage, when the interstitial films are of the order of the bubble diameter (Prud'homme & Khan, 1996), as it will be shown to be the case in my laboratory experiments. The foam drainage reduces the foam height and, when sufficiently efficient, may prevent the foam to become long.

In my laboratory experiments, bubbles are small, hence spherical and non deformable as visually observed. In a natural world, some impurities aggregate at the surface of the rising bubbles, making then similar to rigid particles for modeling the downwards flow of the interstitial liquid (Brennen, 1995; Wallis, 1969). A semi-empirical equation, called the Kozeny equation, is used for complex systems formed with solid particles, and gives very accurate predictions of the drainage velocity U_{Kozeny} (Happel & Brenner, 1973):

$$U_{\text{Kozeny}} = \frac{\rho_{\text{liq}}\, g}{\mu_{\text{liq}}} \frac{(1-\epsilon)^3\, d_{\text{foam}}^2}{36\, \epsilon^2\, k_{\text{kozeny}}} \tag{1}$$

where k_{kozeny}, and d_{foam} are the Kozeny constant, equal to 4.8 (Happel & Brenner, 1973) and 5 is also commonly adopted (Massey, 1989), and the bubble diameter, equal to ≈1.5 mm (Table 1). In the experiments, the gas volume fraction at physical equilibrium ϵ results from a slow accumulation of spheres of equal diameter in a simple cubic packing, hence it is equal to 0.524 (Happel & Brenner, 1973; Vergniolle & Caplan-Auerbach, 2006). For a given particle randomly packed, the gas volume fraction ϵ is approximatively between 0.4 and 0.55 (Massey, 1989).

4.1.2. Theory on the Stability of the Foam in the Reservoir

The behavior of the foam accumulated under a solid roof is controlled by its height. The foam height depends on the balance between the underlying gas flux, which makes the foam thickens, and the foam spreading, which reduces its height by making the foam escapes toward the conduit and it depends on the magma viscosity. However, as the foam grows in thickness, the increasing foam buoyancy leads to the increasing flattening of the bubbles directly below the solid roof. The bubble deformations may become sufficiently large to initiate the massive foam coalescence. At this stage, the foam has become unstable, that is, undergoing massive coalescence events.

The foam stability depends on a dimensionless number N_1, which is the ratio between the maximum foam height h_{m} and its critical height h_{c}, giving (Jaupart & Vergniolle, 1989):

$$N_1 = \left[\frac{3Q_{\text{res}}\mu_{\text{foam}}}{\pi\epsilon_{\text{res}}^2\rho_{\text{liq}}g}\right]^{1/4} \Big/ \left[\frac{4\sigma}{\epsilon_{\text{res}}\rho_{\text{liq}}g d_{\text{res}}}\right] \tag{2}$$

where Q_{res} and ϵ_{res} are respectively the gas flux in the reservoir and the gas volume fraction in the foam in the reservoir, ≈0.6 (Table 1; Table 2).

The foam viscosity μ_{foam} depends on the magma viscosity, μ_{liq} (Jaupart & Vergniolle, 1989):

$$\mu_{foam} = \frac{\mu_{liq}}{(1-\epsilon_{res})^{5/2}}. \quad (3)$$

The ratio between the maximum and the critical foam height, h_{max} and h_{crit}, respectively, is given by (Jaupart & Vergniolle, 1989):

$$\frac{h_{max}}{h_{crit}} = C_{geom}\ N_1 \quad (4)$$

where C_{geom} is a geometrical factor depending on both the radius of the reservoir and that of the conduit, R_{res} and R_{cond}, respectively (Table 1):

$$C_{geom} = \left[-2 \times \ln\left(\frac{R_{cond}}{R_{res}}\right) + \left(\frac{R_{cond}}{R_{res}}\right)^2 - 1\right]^{\frac{-1}{4}} \quad (5)$$

The geometrical coefficient, C_{geom}, labeled 1/A in Equations 32a and 32b (Jaupart & Vergniolle, 1989), is of the order of 1 in the laboratory experiments, hence have been previously ignored in the first study applied to volcanoes (Vergniolle & Jaupart, 1990).

The foam is stable when $N_1/C_{geom} < 1$ (Equations 2 and 5), which corresponds to the weak Strombolian activity displayed by the lava lake at Erta 'Ale (Vergniolle & Bouche, 2016). The foam is unstable for $N_1/C_{geom} > 1$ (Equations 5 and 2) and leads to either the high-level lava fountains for the less viscous magma, such as at Kīlauea and Etna, and Strombolian activity for the more viscous magma, such as at Stromboli (Jaupart & Vergniolle, 1989). The massive foam coalescence is total, that is, removing the entire foam, for the less viscous magma and solely partial for the more viscous magma. Note that N_1 is not very sensitive to the value of the gas flux (Equation 2; Figures 3b and 3c), which is based on gas volume and accurate only to within an error bar of ±20% (see Appendix A for details).

Jaupart and Vergniolle (1989) have checked experimentally that some variation in the bubble diameter does not lead to any major difference in the foam behavior. Therefore I assume in the following that the bubble diameter in the magma reservoir at Shishaldin is the same everywhere at the same depth and is the average value. The differences are also shown to be minor between an inclined and a flat roof (Vergniolle & Jaupart, 1990). Therefore our predictions with this foam model are robust.

The bubble diameter predicted from the foam model for a given underlying gas flux (Equations 2 and 5) is the largest for the largest N_1/C_{geom} and the smallest for the smallest N_1/C_{geom} (Figure 3b). The predicted bubble diameter is also the largest for the smallest viscosity, as shown from comparing the curves labeled Shishaldin (60 Pa.s, Figure 2) and Etna (1 Pa.s, (Giordano & Dingwell, 2003; Métrich et al., 2001; Vergniolle & Gaudemer, 2012)) on one side and Kīlauea (10 Pa.s, (Vergniolle, 2008)) and Erta 'Ale (25 Pa.s, (Vergniolle & Métrich, 2022)) on the other side (Figure 3c).

During the Subplinian phase, the foam accumulated at the roof of the reservoir is in transition between stable and unstable (Figures 1b and 1c). The foam is at its limit of stability for a value of N_1/C_{geom} equal to 1, where C_{geom} (Equation 5) is lying between 0.59 and 0.64 for a surface area of 1 and 0.1 km^2, respectively (Vergniolle, 2008), and a conduit radius of 6 m (Vergniolle et al., 2004). I choose here the largest value of the geometrical factor $C_{geom} = 0.64$ because the magma reservoir is very probably small (Moran et al., 2006) and obtain the threshold value for N_1 of ≈0.64 (Equation 2) above which the foam is unstable.

4.2. Laboratory Experiments

Studies on foams are frequently done using water with a surfactant as the liquid phase, an uncontrolled polydispersed distribution of bubble diameters for the gas phase and a vertical profile in gas volume fraction (Prud'homme & Khan, 1996). However, it is extremely difficult to build a long foam without a surfactant in the liquid, except for highly viscous liquids (Prud'homme & Khan, 1996; Wallis, 1969). Forming a long foam in the conduit, in well-controlled conditions of constant bubble diameter and constant gas volume fraction, is also very rarely achieved in the laboratory. My laboratory experiments here allow to constrain the values to be expected for the initial gas volume fraction, previously unknown when the superficial gas velocity is too large for the foam to be formed at equilibrium. The strength of my laboratory experiments, presented below, is to produce a well-controlled long foam, in conditions likely to approach those prevailing at the beginning of the Subplinian phase. In nature, a certain amount of polydispersivity in bubble diameters is to be expected, even in the top of the magma reservoir. For clarity, I have postponed this discussion to Section 8.

4.2.1. Method and Experimental Set-Up

Laboratory experiments have been performed using an analog volcano, similar to that used to study the foam dynamics on basaltic volcanoes (Jaupart & Vergniolle, 1988, 1989). The apparatus, with a tank and a conduit diameter of 0.28 and 0.044 m, respectively, is filled with a silicone oil (Rhodorsil 47V10), whose viscosity, μ_{liq}, and density, ρ_{liq} are equal to $\approx 9.3 \times 10^{-3}$ Pa.s and ≈ 930 kg.m^{-3}, respectively. The small bubbles were produced at the base of the reservoir by a set of 185 identical capillaries, with a controlled inner diameter of ≈ 0.38 mm, regurlarly spaced. The gas is supplied by a N_2 bottle to prevent gas diffusion into the existing bubbles at a controlled gas flux. The very small diameter of the bubbles compared to that of the conduit ensures that the processes in the conduit are not dependent on the ratio between bubble diameter and conduit diameter, always small.

The specificity of this apparatus, displayed in Figure 4 for a gas flux equal to $\approx 6.7 \times 10^{-6}$ m^3/s, is to be able to produce a population of quasi-identical small bubbles, ≈ 1.5 mm in diameter, within an error of $\leq 10\%$. The characteristics of this regime is to show the existence of a long foam building-up in the conduit in a range of values for the gas flux. When the foam appears in the conduit, the level of its base and top are followed in time by reading values on a ruler glued on the conduit at regular times, indicated by a stopwatch. The laboratory experiments were also photographed with a camera Sony, model DSR-PD170P at set times. The conditions of occurrence of this specific regime and its characteristics have never been explored before.

4.2.2. Dynamic Similarity Between Experiments and Shishaldin

Having both a sufficiently large gas flux and small bubbles within my apparatus is a difficult task, even in the laboratory. The choice of the liquid, the chemistry of gas and gas flux has been driven by the need to fulfill specific requirements, such as not having too large a bubble to ensure that these bubbles are not deformable (Figure 4) and preventing gas diffusion within the foam (Figure 5). I have technical limitations in my apparatus, such as the increase in bubble diameter, hence the bubble deformability, with the liquid viscosity, preventing me to use of a more viscous fluid. The dimensionless analysis of the foam stability and the use of the dimensionless foam height, N_1, clearly show the role of the viscosity on the foam spreading (Equation 2). The chemistry of the gas only plays a role on its ability to diffuse to nearby bubbles. Some gas diffusion exists in the foam growing in the conduit during the pre-Subplinian phase (Vergniolle & Caplan-Auerbach, 2004) but not at a sufficient large rate to prevent the formation of a long foam. In theory, the dimensionless analysis of the foam behavior (Equation 2) can only be applied to volcanic activity if the key parameters of the degassing, magma viscosity, gas flux and bubble diameter, are known independently in the magma reservoir.

The detailed measurements done on the magma composition, temperature and volatile concentration of the melt inclusions (Rasmussen et al., 2018), which are here associated to a model of viscosity reliable for basalts (Giordano et al., 2008a, 2008b), suggest that the magma viscosity at the depth of the reservoir is fairly well estimated (Figure 2). The gas flux there is estimated from its value at the surface and compressed at the depth of the reservoir, making this estimate a reliable one. Estimates on bubble diameters may have been obtained in theory from the measurements of bubble diameters and gas volume fraction in natural pumices at Shishaldin. However, in practice, these studies are rare (Stelling et al., 2002; Szramek et al., 2010). Furthermore, the basaltic pumices evolve after fragmentation due to their low viscosity, preventing the informations on bubble diameter and vesicularity to be representative of that at fragmentation in the conduit (Gardner et al., 1996; Szramek et al., 2010). Additionally, the

bubbles initially in the reservoir are not preserved at the surface because these bubbles escape directly as a gas phase within the eruptive column. Therefore the bubble diameter in the magma reservoir is totally unknown.

Nevertheless, the observation of the eruptive column at the vent is clearly associated to the fragmentation of a long foam accumulated in the conduit, discarding any regime for which the foam at depth is unstable, that is, able to produce series of large bubbles bursting at the vent. Furthermore, the lack of decompression deduced from seismic and infrasonic records (Caplan-Auerbach & McNutt, 2003; Thompson et al., 2002; Vergniolle & Caplan-Auerbach, 2006) discards any mechanism of foam formation in the conduit based on sudden bubble nucleation and growth, making of my model a very well adapted potential mechanism.

4.2.3. Results of the Laboratory Experiments

The small bubbles accumulate at the top of the reservoir as a foam, that is, an assembly of closely packed bubbles (Cantat et al., 2013). The foam thickness results from a balance between its growth produced by the arrival of new bubbles and its spreading, induced by the foam buoyancy, toward the conduit (Jaupart & Vergniolle, 1989; Vergniolle & Bouche, 2016). When the foam is thicker than a critical thickness, it becomes unstable. The massive foam coalescence is then initiated where the foam is the thickest, close to the outer edges of the reservoir (Jaupart & Vergniolle, 1988, 1989). When the foam thickness is just slightly above critical, the coalesced gas pocket, only produced at the outer edges of the reservoir, does not fill the entire surface of the reservoir (Jaupart & Vergniolle, 1989).

I have chosen a set of conditions for which the foam in the reservoir is seen in transition between stable and locally unstable (Figure 5).

When the foam is still thin and stable, its spreading produces a small gas flux toward the conduit (Vergniolle & Bouche, 2016), not sufficient to build a long foam in the conduit (Figure 4). As the foam in the reservoir grows and thickens, its spreading induced by its increasing buoyancy leads to a gas flux sufficiently large to produce a foam continuously growing in the conduit (Figures 6a–6c). This results from the focusing effect of an underlying gas flux produced onto a relatively large surface area, that of the reservoir, within a small conduit. The main condition for building-up a foam in the conduit is to be able to produce a sufficient large gas flux of small bubbles in the conduit to overcome the constant bursting of small bubbles at the top of the conduit. This depends on the underlying gas flux and the ratio of surface areas between that of the reservoir and the conduit. No foam could be built in the conduit when using a larger conduit, with a diameter of 9.4 cm, with the entire range of the experimental gas fluxes. In these conditions, the focusing geometrical effect, with a reservoir radius only three times that of the conduit, is not sufficient to produce a large gas flux in the conduit hence prevents the formation of a long foam. However it is likely that a foam could be formed when using a much larger gas flux. Also note that the interface between the bubbly flow and the foam is very well marked (Figure 6d), as predicted by theory (Wallis, 1969).

When the foam in the reservoir had not yet reached its critical thickness, no local coalescence event can be observed at the top of the reservoir (Figures 5a and 6a). However when the foam starts to become unstable, local small coalescence events occur at the outer edges of the reservoir (Figures 5b and 6b). The resulting gas pockets move toward the conduit together with the foam spreading while new local small coalescence events appear at the outer edge of the reservoir (Figure 5c). This, together with the similar dimension of the coalesced gas pockets (Figure 5), shows that the foam in the reservoir is at the limit between stable, that is, without coalescence events and unstable, that is, undergoing partial or total coalescence. These small coalescence events produce a series of relatively large bubbles, each being equivalent to the formation of a single Strombolian explosion (Jaupart & Vergniolle, 1988, 1989). These voluminous bubbles will exhibit a large overpressure at the vent due to their formation at depth rather than at the surface (Del Bello et al., 2012; Vergniolle, 1998). The first coalesced gas pocket is the exact analogue to the trigger bubble inducing the Subplinian phase (Vergniolle & Caplan-Auerbach, 2004, 2006). The following coalesced gas pockets may appear later in the records or be mostly hidden during the sudden and vigorous foam rupture. Therefore these laboratory experiments show that a foam, trapped at the top of the reservoir and at the limit between stable and unstable regime, is able to reproduce the two of the three main features of the Subplinian phase. The last feature, that is, the sudden disruption of the entire foam trapped in the conduit, not seen in these laboratory experiments, corresponds to the Subplinian phase. Its analysis, which involves a different laboratory apparatus, is the subject of another paper.

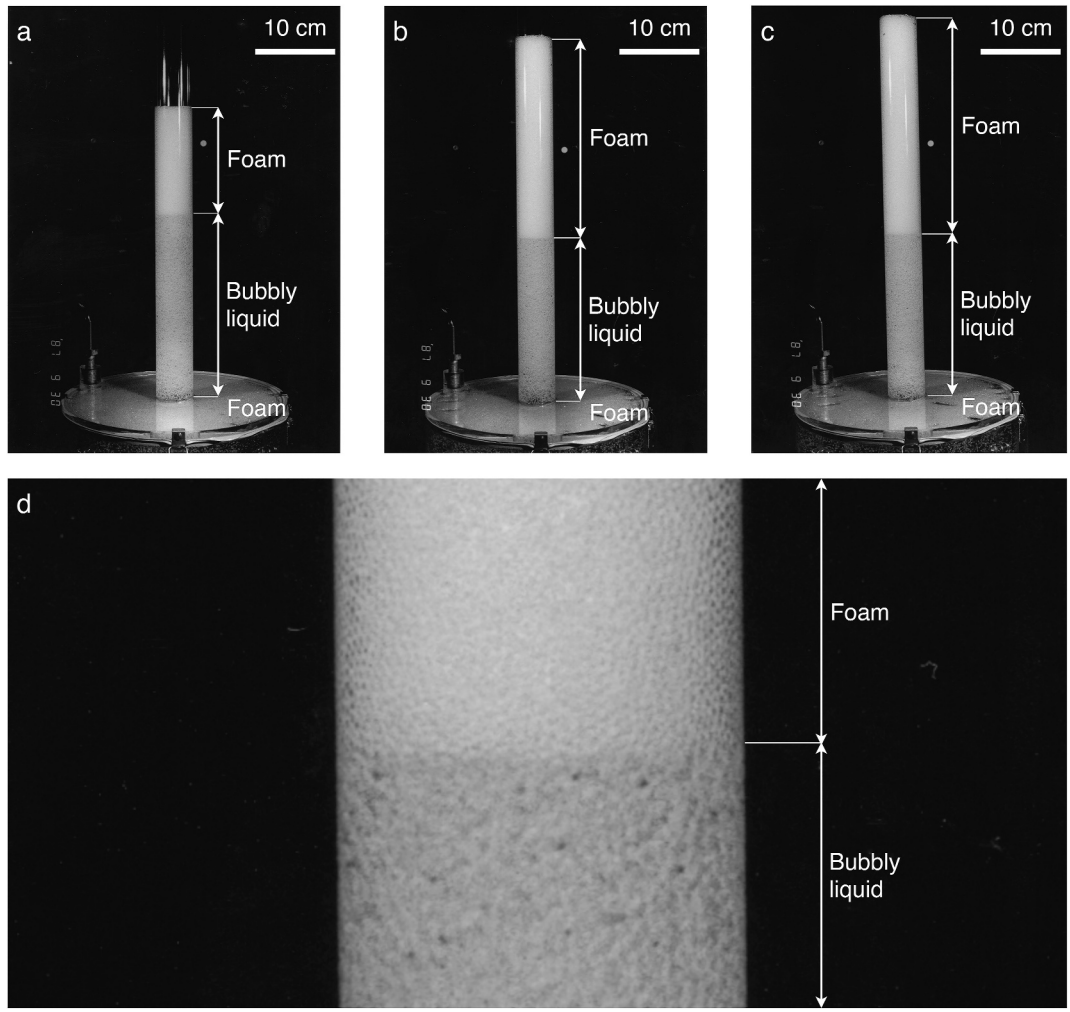

Figure 6. (a, b, c): Full view of the top of reservoir and conduit in the same conditions as in Figures 5a–5c, respectively. The foam (white color) in the conduit is seen growing in time, from ≈13.2 cm (a), 26.4 cm (b) and 29.0 cm (c) in a few tens of seconds, while the foam in the reservoir is in transition from stable (Figure 5a) to just unstable (Figures 5b and 5c). The laboratory experiment was terminated prior to the disruption of the foam in the conduit, thought to be the origin of Subplinian activity; (d) enlargement of the conduit, showing the bubbly liquid, the foam above and the sharp interface between the two, as predicted by theory (Wallis, 1969).

There are only two internal processes, that could reduce the height of a long foam starting to grow in the conduit. The first mechanism is due to the gas diffusion into existing bubbles, leading to the growth of the large bubble at the expanse of the small one, a process called foam ripening. The second mechanism is induced by the drainage by gravity of the interstitial liquid films, when ignoring the effect of any external force, such as a forced shearing or decompression (Neethling et al., 2005; Prud'homme & Khan, 1996).

Firstly, the foam ripening was quasi-suppressed for the duration of my laboratory experiments by using bubbles of quasi-identical diameter (Figure 4) and N_2 as a gas phase, known to diffuse very slowly out of silicone oils. The gas diffusion, if existing, would appear as producing a random polydispersivity in the diameter of the small bubbles within the foam, and bubbles twice as large will be first visible anywhere at the roof of the reservoir. This process is seen to be extremely limited at the roof of the reservoir (Figures 5 and 6d). Note that all large bubbles appearing at the top of the reservoir (Figure 5) are very similar in their gas volumes and clearly located at the outer edges of the reservoir, hence result from the earliest stage of massive foam coalescence rather than gas diffusion.

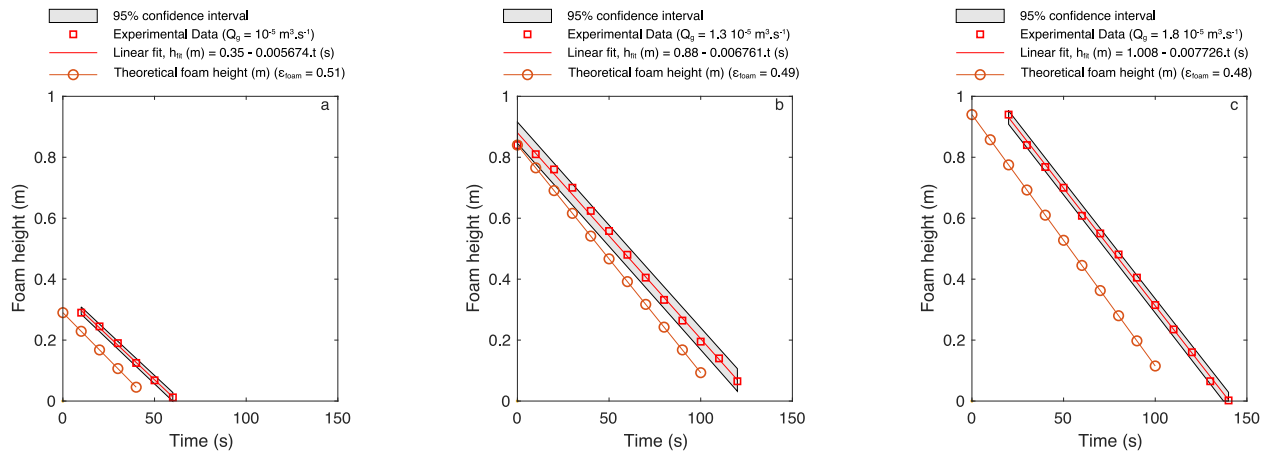

Figure 7. Foam height (m) in time from laboratory experiments in an analog volcano (Figure 6) with conduit diameter of 0.044 m with a silicone oil of viscosity $\approx 9.3 \times 10^{-3}$ Pa.s (Rhodorsil, 47V10) and a foam made with N_2-bubbles of ≈1.5 mm in diameter. Three long foams, 0.29 m, 0.84 m and 0.94 m, have been produced in the conduit under three different values of the underlying gas flux; (a) $\approx 1.0 \times 10^{-5}$ m^3/s; (b) $\approx 1.3 \times 10^{-5}$ m^3/s and (c) $\approx 1.8 \times 10^{-5}$ m^3/s, respectively. When the foam in the conduit is sufficiently long, the gas flux in the experimental reservoir is turned off, which stops the foam from growing at its base. The decrease of the foam height in time (red squares), as the foam is draining, is very linear with drainage velocities of −0.0057 m/s (a), −0.0068 m/s (b) and −0.0077 m/s (c) for an initial gas flux of $\approx 1.0 \times 10^{-5}$ m^3/s, $\approx 1.3 \times 10^{-5}$ m^3/s and $\approx 1.8 \times 10^{-5}$ m^3/s, respectively, as predicted by the Kozeny's equation (Equation 1, blue circles) when using a gas volume fraction in the foam, ϵ, of 0.51 (a), 0.49 (b) and 0.48 (c), respectively, These values are smaller than the equilibrium value, 0.524, showing the departure from equilibrium associated to the fast ascent rate of the bubbles in the conduit of the laboratory experiments. The shaded areas in (a), (b) and (c), which represent the 95% confidence interval from the fit, contain all the experimental data points.

Secondly, the uppermost part of any foam is continuously destroyed because the interstitial liquid films drain under gravity and become too thin to keep the foam structure (Prud'homme & Khan, 1996). Once the drainage is completed, the drained foam at the top disappears, leading to a decrease of the foam height.

Three long foams, 0.29 m, 0.84 m and 0.94 m, have been produced in the conduit under three different values of the underlying gas flux, $\approx 1.0 \times 10^{-5}$ m^3/s, $\approx 1.3 \times 10^{-5}$ m^3/s and $\approx 1.8 \times 10^{-5}$ m^3/s, respectively. When the foam in the conduit is sufficiently long, the gas flux at the base of the reservoir is turned off, which stops the foam from growing at its base. In these conditions, the uppermost part of the foam is destroyed at a rate equal to the drainage velocity, while the liquid, expelled at the foam base, pushes it upwards. Because the gas volume fraction is assumed constant in the foam, a very reasonable assumption due to its mode of formation, the lowermost part of the foam received as much liquid from above than expelled at its base. I cannot visually observe how much liquid is drained at the base of the foam because part of the drained interstitial liquid is simultaneous used to build up new portions of foam. As a result, the foam height decreases at a rate which corresponds to the drainage velocity (Figure 7). In practice, the levels of the base and top of the foam are also changing values due to the escape at the top of the foam of some of the gas previously trapped below the foam in the reservoir and the conduit. However the foam height, measured from the difference between its top and its base, is correctly measured, due to the fast escape of the gas below the foam. Figure 7 shows that the decrease of the foam height in time is very linear. The slope of each fitted straight line indicated drainage velocities of −0.57 cm/s, −0.68 cm/s and −0.77 cm/s for an initial gas flux of $\approx 1.0 \times 10^{-5}$ m^3/s, $\approx 1.3 \times 10^{-5}$ m^3/s and $\approx 1.8 \times 10^{-5}$ m^3/s, respectively. The experimental data points are all contained within the 95% confidence interval (shaded area in Figure 7). I assume that the drainage velocity is estimated within a ±2.5% error bar.

Equation 1 gives a downwards drainage velocity of ≈−0.53 mm/s when using a gas volume fraction of 0.524. This is relatively similar, although slightly lower than that from experiments, −0.57 cm/s, −0.68 cm/s and −0.77 cm/s (Figure 7). The linear decrease of the foam height is very well reproduced by the Kozeny's equation when using a gas volume fraction of 0.51, 0.49, 0.48 for foams initially produced under $\approx 1.0 \times 10^{-5}$ m^3/s, $\approx 1.3 \times 10^{-5}$ m^3/s and $\approx 1.8 \times 10^{-5}$ m^3/s, respectively (Equation 1; Figure 7; Vergniolle, 2024a, 2024b). These values are not far from that predicted for a simple cubic packing, 0.524, and are within the expected values for random packing of similar size particles, 0.4–0.55 (Massey, 1989). The difference between the gas volume fractions estimated during the laboratory experiments with that predicted by the theory, 0.524 at equilibrium, results in the relatively fast accumulation of the small bubbles within the foam and its reduced time available for

drainage. This effect is the largest for the largest gas flux than for the smallest, indicating a departure from the equilibrium value. This result shows that the drainage velocity is well predicted by the Kozeny's equation (Equation 1) and that the real gas volume fraction is not very far from its theoretical value, 0.524, in a foam produced by quasi-identical bubbles.

5. Chronology of Eruption and Its Dynamics

In this section, I apply the theoretical results to the conditions prevailing at Shishaldin, firstly in the foam accumulated in the conduit and secondly in the foam accumulated in the magma reservoir.

5.1. Extent of Foam Drainage at Shishaldin

The hum events, occurring during the pre-Subplinian phase of Shishaldin, have been interpreted as resulting from a shallow foam ripening (Vergniolle & Caplan-Auerbach, 2004, 2006). This interpretation had led to estimate the bubble diameter at the surface of the foam in the conduit between 0.5 and 1.9 mm (Vergniolle & Caplan-Auerbach, 2006). In this case, the maximum drainage velocity obtained when assuming the lowest magma viscosity, that of a melt without crystal existing in the reservoir, ≈60 Pa.s, varies from 1.6×10^{-6} m/s to 1.1×10^{-7} m/s (Equation 1 and Table 2). The existence of the two thermals, that is, small eruptive columns, in the middle of the pre-Subplinian phase suggests that any foam existing in the conduit prior to the two thermals was removed at this time. Hence, it is likely that the foam leading to the Subplinian phase was mostly accumulated in the conduit during the 6 hr separating the end of the two thermals (13:30) and the start of the Subplinian phase (19:31) (Vergniolle & Caplan-Auerbach, 2004, 2006). This interpretation is in agreement with the re-equilibration of the melt inclusions stored in the conduit for durations exceeding hours-days (Rasmussen et al., 2018). The drainage of the foam by gravity (Equation 1) leads to its destruction over a very small height, between 36 and 2.5 mm during the ≈ 6 hr of the foam building-up in the conduit, hence is entirely negligible.

Combining rare coalescence events in the foam in the reservoir with the existence a stable foam in the conduit (Figures 5 and 6) can explain the two of the three main features of the Subplinian activity. Hence, the foam in the conduit at Shishaldin may also result from the dynamics of a foam trapped at the top of the reservoir.

5.2. Stability of the Foam in the Reservoir at Shishaldin

In this section, I apply the theoretical results (Equations 2 and 5) on the foam dynamics (Jaupart & Vergniolle, 1989) to the case of Shishaldin and quantify the bubble diameter in the magma reservoir, d_{res} using the dimensionless foam height N_1 (Equation 2). The foam is at its limit of stability at the initiation of the Subplinian phase and above stability, that is, unstable, during the Strombolian phases. I have used a value for the magma viscosity equal to 60 Pa.s (Figure 2f) and a surface tension of 0.1 kg.s^{-2} as for a wet magma (Gardner & Denis, 2004; Gardner et al., 2013; Khitarov et al., 1979; Mangan & Sisson, 2005) (see Supporting Information S1 for details; Table 2). Results from other choices of parameters are discussed in the section "sensitivity analysis" (Supporting Information S1).

5.2.1. Application to the Subplinian Activity

Using Equation 2 for $N_1 \approx 0.64$ and a gas flux of 0.52 m^3/s just before the Subplinian phase corresponds to a bubble diameter of ≈0.038 mm (Table 2, Vergniolle, 2024a, 2024b). A gas flux of 0.80 m^3/s just before the Subplinian phase, if based on surface activity, corresponds to a bubble diameter of ≈0.034 mm (Table 2). Therefore the choice of the characteristic time during which the foam is built in the reservoir does not change significantly the bubble diameter in the reservoir.

The ideal gas law, applied to spherical bubbles, relates the bubble diameter in the reservoir, d_{res}, to the one at the surface d_{surf} (Table 1) by:

$$d_{surf} = d_{res}\left[\frac{P_{resSub}}{P_{atm}}\right]^{1/3} . \quad (6)$$

The bubble diameters at the surface become ≈0.33 mm and ≈0.29 mm for gas fluxes of 0.52 m^3/s and 0.80 m^3/s, respectively, in reasonable agreement with independent constraints based on foam ripening, between 1.9 and 0.5 mm (Vergniolle & Caplan-Auerbach, 2006).

5.2.2. From Subplinian to Strombolian Activity

The dimensionless foam height N_1 prior to the second Strombolian phase is unknown. However, it is above the value obtained for a stable foam, and possibly similar to that associated to Strombolian phases at Etna, for which $N_1/C_{geom} = 1.2$ (Vergniolle, 2008; Vergniolle & Gaudemer, 2012). Using Equation 2 for $C_{geom} \approx 0.64$, that is, $N_1 \approx 0.76$, and a gas flux of 1.40 m^3/s just before the second Strombolian phase corresponds to a bubble diameter of ≈0.036 mm (Table 2, Vergniolle, 2024a, 2024b). A gas flux of 0.80 m^3/s, if based on surface activity, corresponds to a bubble diameter of ≈0.041 mm (Table 2). Therefore the choice of the characteristic time during which the foam is built in the reservoir does not change significantly the bubble diameter in the reservoir. These estimates of the bubble diameter are minimum values.

Removing a large volume of gas and magma during the Subplinian phase results in a decompression within both the conduit and the magma reservoir and the very likely increase in the bubble diameter within the magma. My laboratory experiments, which are not designed to trigger the sudden foam rupture in the conduit and the resulting decompression, cannot reproduce such a bubble increase, hence to mimic the transition between Subplinian and Strombolian activity.

It is also difficult to be more quantitative on the increase in bubble diameter, obtained after decompression at Shishaldin, because the pressure release is not instantaneous, instead the duration of the pressure release is approximately 47–80 min (Nye et al., 2002; Vergniolle & Caplan-Auerbach, 2006). If the magma removal during the Subplinian phase was instantaneous, the pressure at the base of the conduit would be suddenly decreased by a value corresponding to the weight of a magmatic foam long of 2 km (21 MPa for a gas volume fraction equal to 0.6), suddenly expelled at the surface (Vergniolle & Caplan-Auerbach, 2006). In these conditions, the pressure at the top of the reservoir, approximatively at the lithostatic pressure prior to the Subplinian phase, would largely exceeds that at the base of the conduit, thereby causing the magma to flow from the reservoir toward the conduit. Similarly, the non-instantaneous decompression is likely to have pushed some magma from the reservoir into the conduit, thereby partially restoring some pressure in the reservoir and limiting the increase in bubble diameter. However the fact remains that the bubble diameter in the reservoir must have significantly increased after the Subplinian phase, as an ejecta volume of ≈0.014 km^3 (dense rock equivalent) had been rapidly expelled (Stelling et al., 2002). This is sufficient to make the foam in the reservoir in transition from stable to unstable. Furthermore, the potential increase in the gas flux between the Subplinian and the second Strombolian phase, ≈0.52 m^3/s and ≈1.4 m^3/m^3/s, respectively, if based on the tremor amplitudes, amplifies the foam instability by significantly increasing the foam dimensionless height, N_1, largely above the stability threshold (Equation 2).

5.3. Estimate of the Radius of the Magma Reservoir

The foam accumulated in the reservoir, and at its limit of stability prior to the Subplinian phase, has undergone a very significant pressure release at the end of this phase, likely to have been able to trigger its massive coalescence. I suggest that the first Strombolian phase, only occurring 16 min after the end of the Subplinian phase, results from the withdrawal of the foam trapped in the reservoir. This is in agreement with the marked differences in gas volumes at atmosphere of the two Strombolian phases (Vergniolle et al., 2004), the erratic drops in the tremor amplitudes just before time 20 on Figure 3a and its large gas volume, with a total of $V_{1str} \approx 3.3 \times 10^7$ m^3 (Vergniolle et al., 2004).

For simplicity, I approximate the volume of the foam at the top of the reservoir, V_{foam}, before decompression by its critical volume above which massive coalescence occurs (Jaupart & Vergniolle, 1989), as using the exact shape of the foam at equilibrium only leads to a correction by a factor of ≈0.85 (Vergniolle & Bouche, 2016). I assume that the foam is rectangular, accumulated at a top of a cylindrical reservoir and neglect the small cross section of the conduit (Table 1), giving:

$$V_{foam} = \frac{4\ \sigma S_{res}}{\epsilon_{res}\rho_{liq}\ g\ d_{res}} \quad (7)$$

where S_{res} is the surface area of the magma reservoir. The foam volume is proportional to the gas volume at the depth of the reservoir, V_{gas}, whose changes are related to changes in bubble diameter:

$$V_{gas} = \epsilon_{res} V_{foam} \cdot \tag{8}$$

This yields to a magma reservoir area between 0.13 and 0.12 km^2 when using a gas volume of $\approx 3.3 \times 10^7$ m^3 at the surface (Vergniolle et al., 2004) and compressed at the depth of the reservoir, a gas volume fraction ϵ_{res} of 0.6 and a bubble diameter between 0.038 and 0.034 mm, respectively. This corresponds to an equivalent radius, between 211 and 200 m (Table. 2), respectively, largely exceeding the factor 6 times the conduit radius, ≈6 m (Vergniolle et al., 2004), used by my laboratory experiments. This makes our assumption of a geometrical constriction between reservoir and conduit perfectly valid at Shishaldin, while being in agreement with the interpretation of a small magma reservoir (Moran et al., 2006; Rasmussen et al., 2018). Furthermore the combined use of a foam model, estimates of the gas volumes during the first Strombolian phase with my interpretative view have given an estimate on the radius of the magma reservoir, a parameter rarely known.

If I assume that the height of the reservoir is of the order of its radius, as for Erta 'Ale (Vergniolle & Gaudemer, 2012), the volume of the magma reservoir, assumed to be cylindrical, is estimated to be between 0.025 and 0.030 km^2. This is a minimum value as the magma reservoir can also be a slender body, such as at Etna whose reservoir height is estimated at 3 km (Vergniolle & Gaudemer, 2012). Therefore the volume of the magma expelled during the Subplinian phase, 0.014 km^2, is at most half of that of the magma reservoir, explaining why the 1999 eruption of Shishaldin does not lead to a caldeira collapse.

6. Origin of the Large Gas Flux in the Reservoir

The gas flux Q_{res} in the magma reservoir is the consequence of a population of rising bubbles of diameter d_{res} and a gas volume fraction in the reservoir, α. If the gas volume fraction is sufficiently small, $\alpha \leq 2\%$, the bubbles behave as isolated (Brennen, 2005; Happel & Brenner, 1973) and the gas flux is equal to:

$$Q_{res} = \alpha(1-\alpha)\frac{d_{res}^2 (\rho_{liq} - \rho_{gas})\, g}{18\ \mu_{liq}} S_{res} \tag{9}$$

where ρ_{gas} is the gas density (Table 1), negligible compared to the magma density (Vergniolle & Jaupart, 1990). Bubbles in the magma reservoir of Shishaldin are very small, 0.034–0.038 mm, and are trapped under a relatively small surface area, equal to 0.12–0.13 km^2 (Table. 2). Using Equation 9 and a gas flux equal to 0.52 or 0.8 m^3/s leads to a gas volume fraction exceeding 1, which is impossible by definition.

This suggests that the bubbles at Shishaldin are organized as bubble clusters, which rise much faster than isolated bubbles. Bubbles start to aggregate when the chances of meeting are becoming significant, which occurs as soon as the gas volume fraction exceeds 2% (Brennen, 2005; Happel & Brenner, 1973). I further assume that the bubble clusters are sufficiently small to stay spherical and rise in a laminar regime, that is, driven by a balance between buoyancy and viscous forces. In this case, the velocity of a bubble cluster, U_{clust}, can be calculated by analogy to the velocity of a small bubble, that is, the Stokes velocity, by taking into account that the bubble cluster can be considered as a viscous drop of one liquid, here the bubble cluster with gas volume fraction of ϵ_{clust}, viscosity of μ_{clust} and density, $(1-\epsilon_{clust}) \times \rho_{liq}$, rising into another liquid, referred to with index *liq* (Table 1). This leads to a velocity of U_{clust} equal to (Wallis, 1969):

$$U_{clust} = \left[\frac{g(\rho_{liq} - \rho_{clust})\, d_{clust}^2}{18\mu_{liq}}\right] \times \left[\frac{3\mu_{clust} + 3\mu_{liq}}{3\mu_{clust} + 2\mu_{liq}}\right] \cdot \tag{10}$$

The gas flux can be written by analogy to the rise of a population of isolated bubbles as (Vergniolle & Jaupart, 1990):

$$Q_{gclust} = \alpha_{clust} \times U_{clust} \times S_{res} \tag{11}$$

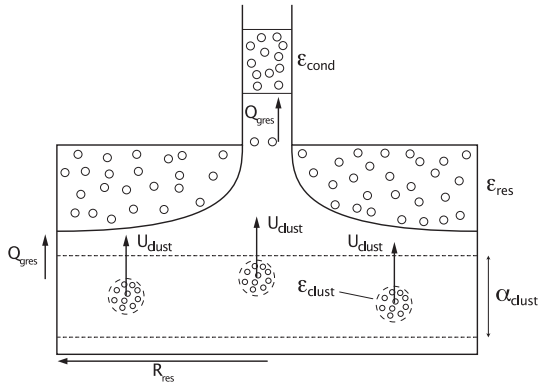

Figure 8. Sketch of a view of the magma reservoir and conduit during the 1999 Shishaldin eruption. The foam in the reservoir, with gas volume fraction ϵ_{res} has reached its equilibrium shape. The underlying gas flux Q_{rges} in the large reservoir is diverted into a small conduit. This favors the formation of a foam in the conduit, with a gas volume fraction ϵ_{cond}, as more gas flux arrives at the bottom of the foam than is destroyed at the top by the hum events during the pre-Subplinian phase. Note that the spreading of the foam toward the conduit makes its innermost part much thinner than its outer region. The gas flux is estimated from the gas volume expelled at the surface and compressed at the depth of the reservoir and a timescale for the foam accumulation. Two estimates of the timescales, prior to the Subplinian and the Strombolian phases, have been discussed, one based on surface activity and the other based on the tremor increase (Figures 3a and Table 2). The large underlying gas flux Q_{gres} is explained by the rise of bubble clusters, with velocity U_{clust} and gas volume fraction ϵ_{clust}, arriving as a population of bubble clusters with a gas volume fraction α_{clust}, assumed to be between 0.63% and 2% (Brennen, 2005; Happel & Brenner, 1973). The early formation of the bubble clusters by hindering the bubble growth by gas diffusion can explain the tiny bubble diameter found at Shishaldin.

where α_{clust} is the gas volume fraction of the bubble clusters, considered as drops of a different fluid (Figure 8). I also assume that the gas volume fraction of the bubble clusters, α_{clust}, is equal to the upper limit of the diluted regime, because any excess bubble is preferably used to increase the diameter of the existing bubble cluster nearby rather than producing a new bubble cluster. The proposed limits of the diluted regime are 0.63%–2% (Happel & Brenner, 1973) and 1%–2% (Brennen, 2005), values which correspond to the threshold above which the bubbles are seen interacting together. Therefore the diameters of the bubble clusters prior to the Subplinian phase, d_{clust} are equal to ≈3.5 mm and ≈4.6 mm, when assuming an underlying gas flux of 0.52 m^3/s and 0.80 m^3/s, respectively, for a gas volume fraction of 2% and a reservoir radius of ≈200 m (Table. 2).

The Reynolds number of a bubble cluster, the ratio between inertia and viscous forces, is adapted to that of a single bubble (Brennen, 1995) by using the upwards velocity of the bubble cluster and its diameter:

$$Re_{clust} = \frac{\rho_{liq} U_{clust} d_{clust}}{\mu_{liq}} \quad (12)$$

giving a value $\lesssim 4.0 \times 10^{-4}$ for all diameters (Table 2). This largely supports the assumption of a laminar rise.

The same reasoning can be applied to the diameter of the bubble clusters prior to the second Stombolian phase (Equations 10 and 11). The diameters of the bubble clusters are equal to 5.7 and 4.6 mm, for a gas flux based on tremor records (1.4 m^3/s) and that based on surface activity (0.8 m^3/s), respectively, (Table. 2).

These large bubble clusters, with a diameter larger than two orders of magnitude than that of the sole bubble, contains numerous bubbles (Table 2). Most of the bubbles within the bubble cluster are only in contact with thin interstitial films, which can be easily be depleted in volatiles. This, added to the fast rise of the bubble clusters, hinders significantly the gas diffusion into the bubbles, even for the fast-diffusing H_2O phase. The consequence is that the bubble growth after the formation of the bubble clusters mostly occurs by decompression, hence by rising, rather than by gas diffusion. This is atypical because so small a bubble should be mostly growing by gas diffusion, a very efficient process at this stage of the bubble growth (Lensky et al., 2004). This hindered gas diffusion toward the existing bubbles can explain the unusual small bubble diameter.

Here a new degassing mode had been proposed for the magma reservoir, which meets the two conditions of a very small bubble diameter with a large gas flux. The large underlying gas flux in the reservoir promotes a very large gas flux at the base of the conduit, necessary to build a foam, while the very small bubble diameter ensures that the liquid drainage within the foam is negligible (Equation 1), making the foam able to grow to a length of ≈2 km (Vergniolle & Caplan-Auerbach, 2006). Hence, these two conditions are simultaneously required to initiate the formation of a long foam in the conduit, whose collapse by an additional mechanism, not discussed here, will lead to the high-level eruptive column of the Subplinian phase.

7. Sensitivity of the Results

I have run a sensitivity analysis on the results of the models by selecting the entry parameters for the foam drainage and for the degassing magma reservoir and using a random sampling of a quasi-Gaussian distribution with a Monte-Carlo analysis. I have truncated a few initial Gaussian distribution to remove unrealistic or negative values on some physical parameters, whenever necessary.

Firstly, I have applied this method to the laboratory experiments on the foam drainage (Figure 7) and on the experimental determination of the gas volume fraction within the foam. The errors on the entry parameters are very small, ±2.5% error on liquid viscosity and density and on the drainage velocity, ±5% error on the bubble

diameter. The Kozeny constant had been made to vary between the two extreme values given in the literature (Happel & Brenner, 1973; Massey, 1989). The gas volume fraction is predicted with a very small standart deviation of ±0.02 for a mean value between 0.48 and 0.51, showing that the predictions of the model are very robust (Figure S1).

Secondly, I have applied the same method to the estimate of the entry parameters for the model on the behavior of the degassing magma reservoir (Figure S2). I have chosen a magma viscosity, density and surface tension among values such as, 105 ± 45 Pa.s (Figure 2; Mader et al., 2013), 2,600 ± 100 kg.m^{-3} (Stelling et al., 2002) and 0.1 ± 0.02 kg.s^{-2} (Gardner & Denis, 2004; Gardner et al., 2013; Khitarov et al., 1979; Mangan & Sisson, 2005; Proussevitch & Kutolin, 1986; Walker & Mullins, 1981), respectively. The gas volume fraction of the bubble clusters, inside the bubble clusters and in the foam are assumed to vary between 0.013 ± 0.0069, 0.524 ± 0.048 and 0.524 ± 0.048, respectively. The gas volume at the surface prior to the Subplinian phase and the first Strombolian phase are taken to be $8.0 \pm 1.6 \times 10^7$ m^3 (Appendix A) and $3.3 \pm 0.5 \times 10^7$ m^3, respectively (Figure 1), while the pressure of the magma reservoir and its geometrical coefficient lie within $6.7 \pm 0.7 \times 10^7$ Pa and 0.63 ± 0.01, respectively. The bubble diameter in the reservoir and that at the surface were predicted to be $4.3 \pm 1.3 \times 10^{-5}$ m and $3.7 \pm 1.1 \times 10^{-4}$ m, respectively, while the diameter of the bubble clusters and the radius of the reservoir were estimated at $7.2 \pm 5.2 \times 10^{-3}$ m and 207 ± 33 m, respectively, (Figure S2). The small standart deviations obtained on the results show that the modeling is very robust, despite uncertainties in the entry parameters.

8. Discussion

I have so far proposed that the Subplinian phase results from the spreading of a foam accumulated in the reservoir and at the transition between stable and unstable. My predictive model can constrain the average bubble diameter in the reservoir but cannot take into account a distribution in bubble diameter, as processes related to the instability are already difficult to solve for a sole bubble diameter. The existence of a polydispersed suspension of bubble diameters make the gas volume fraction within the foam, equal to ≈0.524 for a very narrow distribution and 0.62 for a wider distribution (Happel & Brenner, 1973). By using a gas volume fraction of 0.6 in the foam at Shishaldin, I have implicitly assumed that the bubbles in the foam did not have exactly the same diameter. If the bubbles are markedly different in diameter and in sufficient amount, the bubble coalescence in the foam is mostly driven by the largest ones, which are the first to be deformed and ruptured (Jaupart & Vergniolle, 1989). In this case, the smallest bubbles can be considered as inducing a viscosity increase, which depends on their gas volume fraction (Mader et al., 2013). Furthermore, the amount of polydispersivity at Shishaldin is probably relatively reduced because (a) the bubbles are very small hence unlikely to coalesce together due to their large inner capillary pressure, (b) are organized as bubble clusters very early after nucleation, hence grow mostly by decompression due to their large rise velocity, and (c) the residence time of the foam at the top of the magma reservoir is small, only of a few days if based on the tremor increase on April 17 and less if based on surface activity. In the absence of further constraints on the distribution in bubble diameters, I cannot go further in assessing the errors of my simplified model.

8.1. Basaltic Eruption Dynamics From Conduit Processes

During explosive eruptions, transitions between explosive and effusive phases are frequent (Sparks et al., 1997). These transitions have been explained by magma losing gas to fractured country rock during its ascent toward the surface (Jaupart & Allègre, 1991; Woods & Koyaguchi, 1994). Eruptive behavior is very sensitive to eruption rate and to changes in reservoir pressure which in turn result in changes in flow regimes. However at Shishaldin, there is evidence of degassing prior to and during the Subplinian phase (Rasmussen et al., 2018; Stelling et al., 2002), and a lack of deformations in the edifice prior to the eruption (Lu & Dzurisin, 2014; Moran et al., 2006), which discards a mechanism based on gas loss through the conduit walls.

The fragmentation mechanism upon decompression is fondamentally different for a low-viscosity bubbly basalt than for a high-viscosity silicic magma (Namiki & Manga, 2006). The fragmentation of a basaltic melt is entirely driven by fluid mechanics and by a critical Reynolds number of the order of 1 below which the foam in the conduit remains stable and the degassing is not that of a fragmenting foam (Namiki & Manga, 2006).

In an alternate model of basaltic eruptions (Parfitt, 2004; Parfitt & Wilson, 1995), the magma ascent velocity has been taken as the key parameter to explain the occurrence at the surface of a gas-rich eruptive phase. When the magma velocity is large, the bubbles cannot move relative to the magma and a region with a very high gas content

develops in the conduit. Fragmentation of that "foam" (gas volume fraction from 60% to 95%) combined with gas expansion produces the observed high-level lava fountains (Parfitt, 2004; Parfitt & Wilson, 1995). In contrast, Strombolian explosions are explained by progressive and repetitive coalescence events in the conduit, due to a lower magma rise speed (Parfitt, 2004; Parfitt & Wilson, 1995).

Parfitt (2004) distinguishes a new class of basaltic eruptions in which Strombolian explosions give way to high-level lava fountains. Several eruptions of Etna show this feature (e.g., Allard et al., 2005). Parfitt (2004) explains that regime by a magma rise speed intermediate between the large velocity leading to high-level lava fountains and the low velocity responsible for Strombolian explosions. However more recent chemical gas measurements obtained at the vent on 14 June 2000 shows that the high-level lava fountains at Etna results from a massive coalescence of a foam layer trapped at ≈1.5 km depth below the summit (Allard et al., 2005; La Spina et al., 2015; Spillaert et al., 2006). Furthermore seismic waveforms recorded during the 2001 eruption at Etna are well explained by a model based on a foam collapsing at a structural barrier (Gresta et al., 2004).

At Stromboli, the tremor ground displacement is best explained by a foam coalescence trapped at a structural barrier (Ripepe & Gordeev, 1999), later confirmed by gas measurements (Burton et al., 2007). The broadband seismic signal and the short periods (≥1 s) are also very well reproduced by laboratory experiments of a foam collapse previously accumulated at the top of the reservoir (Ripepe et al., 2001). This is another result in favor of a model based on foam dynamics (Jaupart & Vergniolle, 1988, 1989; Vergniolle & Jaupart, 1990).

Basaltic Subplinian eruptions have not been considered by the eruption models based on changes of rise speed (Parfitt, 2004; Parfitt & Wilson, 1995), probably because such events are rare. La Spina et al. (2021) have proposed a detailed parametric study, in which the outgassing, magma ascent rate and rheology in the conduit were tuned in to explain both high-level lava fountains and eruptive columns at basaltic eruptions. They calculate a criteria for fragmentation and assumed that high-level basaltic columns are associated to a brittle fragmentation. They show that the range of parameters leading to high-level eruptive columns, assumed to be due to closed-system degassing, was less restricted for Etna than for Kīlauea. However at Shishaldin, the fragmentation occurred in a ductile regime (*Stelling*, pers.com.), in agreement with the lack of initial overpressure at its initiation and the coarse-grain deposits not distinguishable from the Strombolian deposits (Stelling et al., 2002). Furthermore the degassing does not occur as a closed-system, as for explosive volcanoes for which the fragmentation is brittle, but as an open-system degassing (Rasmussen et al., 2018; Stelling et al., 2002), preventing the use of La Spina et al. (2021) 's model for Shishaldin.

The eruptive activity at Shishaldin is fundamentally different from Kīlauea, with small ash plumes being the norm at Shishaldin and high-level lava fountains the norm at Kīlauea. The difference in viscosity at the depth of the magma reservoir is not very large between Kīlauea, ≈10 Pa.s (Vergniolle & Gaudemer, 2012) and Shishaldin, ≈60–150 Pa.s (Figure 2f), hence a fine tuning is needed if the *Parfitt*'s model, (2004), is used to explain both basaltic high-level eruptive columns and high-level lava fountains.

Although eruptions with high-level eruptive columns are not considered typical of basaltic volcanoes, the typical delay between eruptions at Shishaldin (Beget et al., 1998; Nye et al., 2002) is similar to that of a classical basaltic eruptions elsewhere, suggesting indeed that a single mechanism should explain any type of basaltic activity, despite their very different surface activity. In my views, the strength of a model based on the foam dynamics (Jaupart & Vergniolle, 1988, 1989; Vergniolle & Jaupart, 1990) lies in its ability to explain four very different eruptive regimes at the surface by simple changes of the conditions in the reservoir, namely gas flux, magma viscosity and bubble diameter.

Furthermore my model is only based on two conditions, which are easily met on basaltic volcanoes, that is, the existence of a reservoir whose radius is at least three to six times that of the conduit and gas saturation in the magma reservoir. The detailed mechanism by which a long foam accumulated in a conduit can be ruptured to produce a high-level eruptive column is the subject of another study, involving a different laboratory apparatus.

8.2. Comparison of Degassing Patterns on Other Volcanoes

8.2.1. Constraints Brought by the Foam Dynamics in the Magma Reservoir

The four eruptive regimes at basaltic volcanoes are the weak Strombolian activity such as at Erta 'Ale, the high-level lava fountains such as at Etna and Kīlauea, the typical Strombolian activity such as at Stromboli and the

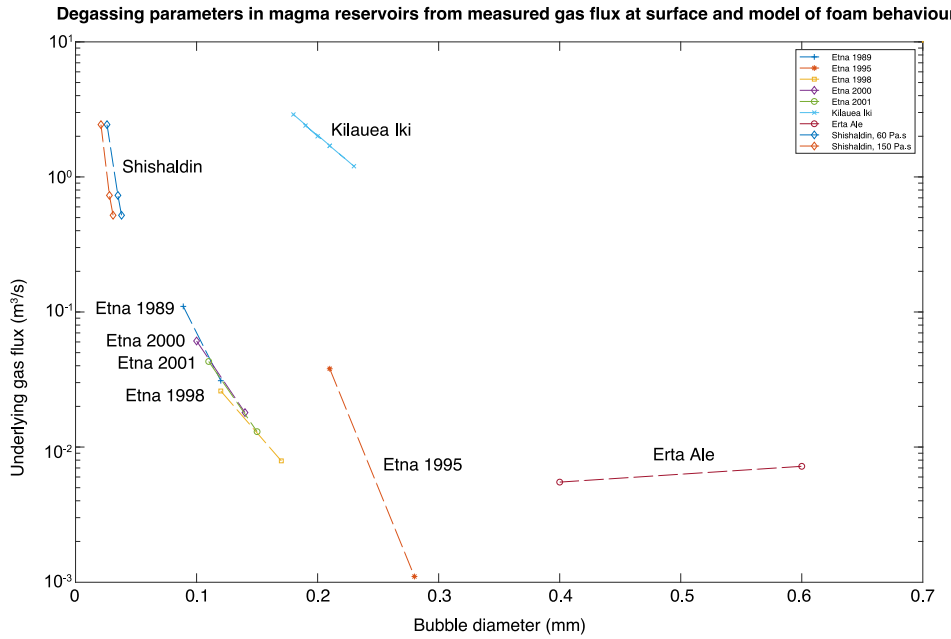

Figure 9. Underlying gas flux (m^3/s) at the top of the reservoir as a function of the bubble diameter (mm) in the reservoir for 5 eruptions at Etna (1989, 1995, 1998, 2000, 2001), the Kīlauea Iki eruption, at Erta 'Ale and Shishaldin using the foam model and the expelled gas flux (Vergniolle, 2008; Vergniolle & Bouche, 2016; Vergniolle & Gaudemer, 2012). The bubble diameter was overestimated during the 1995 eruption at Etna due to an underestimation of the gas flux, making the degassing parameters at the 5 eruptions of Etna more similar to one another. Magma viscosities were 10 Pa.s for Kīlauea (Vergniolle, 2008), 1 Pa.s for Etna (Giordano & Dingwell, 2003; Métrich et al., 2001; Vergniolle & Gaudemer, 2012), 25 Pa.s at Erta 'Ale (Vergniolle & Métrich, 2022) and 60–150 Pa.s for Shishaldin (Figure 2f). Surface tensions were 0.36 kg.s^{-2}, 0.10 kg.s^{-2}, 0.36 kg.s^{-2} and 0.1 kg.s^{-2} at these four volcanoes, respectively. The gas volume fraction at Erta 'Ale is extremely small, 0.023%–0.063% (Vergniolle & Bouche, 2016), small at Etna, 0.018%–1.2% (Vergniolle, 2008; Vergniolle & Gaudemer, 2012), large for the Kilauea Iki eruption at Kīlauea, ≥2% (Vergniolle, 2008), and Shishaldin ≥2%, leading to the formation of bubble clusters (Figure 8). The radius of the reservoir is the smallest at Erta 'Ale, relatively small at Etna and Shishaldin, and the largest for the Kīlauea Iki eruption, with radii of 155–170 m, 260–300 m, 200–210 m, 420–780 m, respectively (Vergniolle, 2008; Vergniolle & Bouche, 2016). Note that Etna has degassing parameters in the reservoir relatively close to that of Shishaldin, as expected from its 1.8% of Etna eruptions being Subplinian (Coltelli et al., 1995, 2000). The difference between the bubble population at these four volcanoes is explained by a different magma ascent rate, very large at Shishaldin, large at Kīlauea, intermediate at Etna and small at Erta 'Ale.

high-level eruptive columns such as at Shishaldin. All these patterns can be explained by the accumulation of a foam at the top of the reservoir, which is stable for weak Strombolian activity (Vergniolle & Bouche, 2016), unstable for high-level lava fountaining and typical Strombolian activities (Jaupart & Vergniolle, 1988, 1989; Vergniolle, 2008; Vergniolle & Gaudemer, 2012; Vergniolle & Jaupart, 1990) and at the limit between stable and unstable at Shishaldin.

The bubble diameter and the radius of the reservoir have been deduced at Erta 'Ale, Etna and Kīlauea from the gas flux measured at the surface, the reservoir depth and the foam model (Figure 9). These results were obtained in the same conditions as for modeling the magma reservoir at Shishaldin, using a gas volume fraction of 0.6. This corresponds to the lowest estimate for the bubble diameter (mean −1 standard deviation) and the mean value for the radius of the magma reservoir. Note that the 1995 eruption at Etna occurred at a different vent (northeast crater) than the rest of the eruptions (southeast crater). Furthermore, the gas flux in 1995 was significantly underestimated and not as accurately estimated as for the rest of the eruptions (Vergniolle & Gaudemer, 2012). This had led to an overestimate on the bubble diameter in 1995, making all the five eruptions at Etna resembling to one another (Figure 9).

The underlying gas flux is among the smallest at Erta 'Ale (Vergniolle & Bouche, 2016) and among the largest at Shishaldin and for the Kilauea Iki eruption Kīlauea (Vergniolle, 2008; Vergniolle & Jaupart, 1990) (Figure 9). In constrast, the bubble diameter is the smallest at Shishaldin, intermediate at Etna and for the Kilauea Iki eruption Kīlauea and the largest at Erta 'Ale (Figure 9). The gas volume fraction at Erta 'Ale is extremely small, 0.023%–

0.063% (Vergniolle & Bouche, 2016), small at Etna, 0.018%–1.2% (Vergniolle, 2008; Vergniolle & Gaudemer, 2012), large for the Kilauea Iki eruption at Kīlauea, ≥2% (Vergniolle, 2008), and Shishaldin ≥2%. The radius of the reservoir is the smallest at Erta 'Ale, relatively small at Etna and Shishaldin, and the largest for the Kīlauea Iki eruption, with radii of 155–170 m, 260–300 m, 200–210 m, 420–780 m, respectively (Vergniolle, 2008; Vergniolle & Bouche, 2016).

Other estimates on the radii of the reservoir are comparable to our estimates based on the foam dynamics at Etna, where the degassing reservoir is small (Albarède, 1993; Calvari et al., 2001) and ≈0.5 km^3 (Condomines & Michaud, 1995; Le Cloarec & Pennisi, 2001), hence with an equivalent spherical radius of ≈500 m, and that at Kīlauea, ≈500 m (Yang et al., 1992). The magma reservoir is suspected to be small at Shishaldin (Moran et al., 2006; Rasmussen et al., 2018), which is in perfect agreement with a radius of ≈200 m, hardly detectable on deformations.

The relatively small radius of the shallow magma reservoir may imply a relatively small magma reservoir with a height of the order of the diameter, such as at Erta 'Ale with a reservoir thickness of 150–240 m. But it may also correspond to a relatively large magma reservoir, with a height exceeding 3 km, such as at Etna (Vergniolle & Gaudemer, 2012). The small surface area or its slender shape can explain why shallow magma reservoirs are difficult to be detected by geophysical measurements. The example of Shishaldin also shows the role of the reservoir radius onto the degassing pattern. The combinaison of a small radius with a relatively large gas flux implies the formation of bubble clusters within the reservoir (Figure 8; Equations 10 and 11; Table 2). However, bubble clusters can also be formed in a magma reservoir with a large surface area, such as during the Kīlauea Iki eruption. The diameters of the bubble clusters during this eruption, between 0.7 and 2.3 mm (Equations 10 and 11), are smaller than those at Shishaldin (Table 2), due to the large surface area of the reservoir.

At Shishaldin, the typical bubble diameter in the reservoir, between 0.038 and 0.034 mm, although small, is above the critical bubble diameter at nucleation, ≤0.1 μm (Sparks, 1978; Sparks et al., 1994) and now approximately estimated to be a few nanometers (Mourtada-Bonnefoi & Laporte, 2002). This bubble nucleus can grow very rapidly to 1–10 μm as the gas diffusion is extremely efficient for so small a bubble (Hamada et al., 2010), larger values, such as 10–100 μm for rhyolitic melts (Lyakhovsky et al., 1996) and 10–50 μm for basaltic melts such as at Stromboli (Pichavant et al., 2013), resulting from a quasi-instantaneous bubble growth after nucleation. Hence the bubbles at Shishaldin nucleated and hardly grew in the reservoir before the eruption. This is in very good agreement with the existence of bubble clusters, whose bubble growth by gas diffusion is limited by both their fast ascent velocity and by the small thickness of the interstitial films, rapidly depleted in volatiles (Figure 8). The tiny bubble diameter at Shishaldin is smaller than the vesicle diameter of the Kīlauea submarine basalts, ≈0.1 mm (Moore, 1965), which are erupted at a depth of 4–5 km, hence at a pressure closer to the shallow magma reservoir than that of pumices collected at the vent (Vergniolle & Jaupart, 1990). It is also smaller than the diameter of the bubbles collected within the glasses from mid-oceanic ridge basalts, 0.05–0.2 mm (Chavrit et al., 2012). Bubble diameter at Shishaldin is also smaller than that at Erta 'Ale, 0.4–0.6 mm (Vergniolle & Bouche, 2016) and for the Kilauea iki eruption at Kīlauea, ≈0.2 mm (Vergniolle, 1996, 2008; Vergniolle & Jaupart, 1990), which are both close to predictions of a model for bubble nucleation and growth in dry basaltic melts (Bottinga & Javoy, 1989, 1990).

The differences in the diameter of the bubble clusters and that of the bubbles, twice as large and six times smaller, respectively, at Shishaldin than during the Kīlauea Iki eruption, suggests that the formation of the bubble clusters during the Kīlauea Iki eruption does not occur as early after the bubble exsolution than during the 1999 eruption at Shishaldin. The very early formation of the bubble clusters at Shishaldin is in agreement with a deep exsolution of CO_2, as already proposed at Sunset crater (≈6,000 ppm, (Allison et al., 2021)), due to the relative richness in CO_2 of the magma at Shishaldin (≈2,700 ppm, (Rasmussen et al., 2018)) when compared to that during the Kīlauea Iki eruption (≈400 ppm, Ferguson et al., 2016)).

8.2.2. Origin of the Bubbles in the Magma Reservoir

The bubble number density, that is, the number of bubbles in a reference volume, can be deduced directly from the gas volume fraction when the bubbles are isolated. It can also be deduced from the diameter of the bubble clusters, the largest bubble clusters indicating the largest initial bubble number density, when assuming a smilar gas volume fraction, here between 0.63% and 2%. Therefore the bubble number density in the magma reservoir is maximum at Shishaldin, large for Kīlauea Iki, intermediate at Etna and small at Erta 'Ale. This is in agreement

with the bubble number densities found in the pyroclasts ejected during the 122 BC eruption at Etna, 10^6–10^8 cm^{-3}, and those at Tarawera, 10^6 cm^{-3}, which are 1–2 orders of magnitude higher than those obtained in typical Strombolian and Hawaiian scoria (Sable et al., 2009).

The bubble number density had been used to estimate the magma ascent rate by using a model based on the diffusivity of H_2O (Toramaru, 1995) for explosive eruptions (Toramaru, 2006). This model had also been adapted to the diffusivity of CO_2 to asses the decompression rate, that is,.magma ascent rate, at the mid-oceanic ridges basalts (Chavrit et al., 2012). These calculations showed that a large bubble number density is indicative of a large ascent rate whereas a small bubble number density corresponds to a small ascent rate. Laboratory experiments made by decompressing a silica-rich magma containing water have also shown that the bubble nucleation depends on the decompression rate. A fast decompression rate leads to a population of numerous and small bubbles, whereas a slow ascent rate leads to less numerous but larger bubbles (Hamada et al., 2010; Mourtada-Bonnefoi & Laporte, 2004). In these conditions, it is tempting to associate the very large bubble number density at Shishaldin to a very fast magma ascent rate, as already qualitatively proposed (Stelling et al., 2002), the large bubble number density during the Kīlauea Iki eruption to a large ascent rate, to suggest an intermediate ascent rate at Etna and a slow ascent rate at Erta 'Ale.

This is in agreement with the estimates of magma ascent rate at Kīlauea, with 17 m/s for the 10-km high Subplinian column (ca. 1650) and 2 m/s for the high-level lava fountains of Kīlauea Iki eruption (Ferguson et al., 2016), that for the Subplinian phase of Fuego in 1974, 8–21 m/s (Llyod et al., 2014) and with the small values found for the ascent rate for the basalts emitted at the mid-oceanic ridges, between 0.019 m/s and 0.88 m/s (Chavrit et al., 2012). The magma ascent rate had been estimated from bubble number density and the textures of the samples, at 1–2 m/s for the paroxysmal activity at Stromboli (Pichavant et al., 2013, 2022) and at 53 m/s for the mafic Curacautín ignimbrite at Llaima (Valdivia et al., 2022). Similarly, it had been estimated to be between 3.8 m/s and 7.6 m/s and between 0.19 m/s and 3.8 m/s at Masaya (Fontana lapilli) and Shishaldin, respectively (Szramek, 2016). The magma ascent rate, estimated from the bubble number density, is only known with ± one order of magnitude (Chavrit et al., 2012). Furthermore, the laboratory experiments, done by decompressing a basalt containing both CO_2 and H_2O, have shown that the homogeneous bubble nucleation is relatively continuous, in contrast to the bubble nucleation in a magma presenting only one volatile phase, here a basaltic melt rich in H_2O (Le Gall et al., 2016a, 2016b; Pichavant et al., 2013) or that of a rhyolitic melt with both CO_2 and H_2O (Mourtada-Bonnefoi & Laporte, 2002). While it is likely from the bubble number density that the magma ascent rate is the largest for Shishaldin, large for the Kilauea iki eruption at Kīlauea, intermediate at Etna and small at Erta 'Ale, it is difficult to be more quantitative at this stage. Therefore, the bubble number density at these four volcanoes, hence the population of small bubbles, is likely to mainly result from different magma ascent rates in the magma reservoir.

8.2.3. Eruptive Patterns From Degassing Magma Reservoir

The difference between the high-level lava fountains during the Kīlauea Iki eruption and the Subplinian activity at Shishaldin is a direct consequence of the difference in the bubble diameter in the reservoir, six times smaller at Shishaldin than at Kīlauea (Figure 9). The difference between the high-level lava fountains at Etna and the Subplinian activity at Shishaldin results from both the underlying gas flux, smaller at Etna than at Shishaldin, and the bubble diameter, larger at Etna than at Shishaldin (Figure 9). It is also important to notice that a stable foam accumulated in the reservoir can lead to two very contrasted eruptive regimes, the weak Strombolian activity, such as at Erta 'Ale, or the Subplinian activity such as at Shishaldin, the difference being in both the underlying gas flux and the bubble diameter (Figure 9). The similarity in reservoir radii at Erta 'Ale and Shishaldin, only larger by 20% in radius, suggests both eruptive regimes, that is, due to an almost stable foam, are obtained by two very contrasted bubble populations, numerous tiny bubbles at Shishaldin and fewer and bigger bubbles at Erta 'Ale (Figure 9). It is also important to note that the large underlying gas fluxes for the Kilauea Iki eruption at Kīlauea is mostly obtained by a larger reservoir radius, twice as large in radius, hence larger by a factor 4 in surface area, than that at Shishaldin, and mostly by a larger gas volume fraction at Shishaldin than for the Kilauea Iki eruption at Kīlauea (Equation 11).

My study shows that the Subplinian activity at Shishaldin results from both a very large underlying gas flux and a very small bubble diameter when compared to other basaltic volcanoes (Figure 9). This induces the foam trapped at the top of the reservoir to be at its limit of stability at Shishaldin, thereby focusing a large gas flux into a much

smaller conduit, a configuration for which a foam can grow into the conduit and be disrupted within a high-level eruptive column. In this paper, I have proposed a basis to draw a diagram for all basaltic eruptive regimes, only using bubble diameter, magma viscosity and gas flux in the magma reservoir (Figure 9). In the future, more studies are needed to better define the limit between eruptive regimes.

9. Conclusion

Infrasonic measurements, by leading to estimates of the expelled gas volumes during each stage of the eruption, had provided a quantitative understanding of the eruption dynamics for a large basaltic eruptive column, solely based on the dynamics of the foam layer trapped at the top of the reservoir. The quantification of the underlying gas flux in the reservoir was deduced from the gas volume expelled during each phase of eruptive activity and from a timescale for foam accumulation at the top of the reservoir. Two different timescales were used, one based on the temporal evolution of the RMS seismic amplitudes and one based on surface activity, giving underlying gas fluxes of ≈0.52 m^3/s and ≈0.73 m^3/s, respectively. The use of estimates of magma composition and temperature obtained from melt inclusions (Rasmussen et al., 2018) combined with a model for the viscosity (Giordano et al., 2008a, 2008b) has given a quantitative estimate of the magma viscosity with depth.

Laboratory experiments have shown that a foam in the reservoir at its limit of stability could lead both to the formation of a long foam in the conduit, whose sudden rupture not studied here was at the origin of the Subplinian eruptive column, and to the formation of a large gas pocket, analog to the trigger bubble, thought to be responsible for this foam rupture at Shishaldin. The use of the dimensionless foam height, N_1 (Equation 2), for the foam in the reservoir and interpreted to be that at the transition between stable and unstable foam gives an estimate of the bubble diameter in the reservoir of ≈0.038 mm and ≈0.034 mm, when combined with the underlying gas fluxes prior to the Subplinian phase of 0.52 m^3/s and 0.80 m^3/s, respectively.

The strong decompression induced in the bubbly magma, by the removal of a large quantity of gas and liquid during the Subplinian phase, is thought to be responsible for the coalescence of the remaining foam in the reservoir, at the origin of the first Strombolian phase. This expelled gas volume, once compressed at the depth of the reservoir, is combined with the theoretical volume of a quasi-stable foam in the reservoir produced by the underlying gas flux prior to the Subplinian phase, to estimate the radius of the reservoir. Its small dimension, 200–210 m, is sufficiently small to explain the lack of deformations prior to the Subplinian activity (Moran et al., 2006; Rasmussen et al., 2018).

The large underlying gas flux, between 0.52 m^3/s and 0.80 m^3/s, can not be explained by the rise of a diluted population of tiny bubbles, such as with a diameter of 0.038–0.034 mm. Hence, these bubbles must be so numerous that they are organized into fast-rising bubble clusters very early after nucleation and when their gas volume fraction becomes above the threshold between diluted and non-diluted regimes, between 0.63% and 2% (Brennen, 2005; Happel & Brenner, 1973). I had assumed that the diameter of the bubble clusters is such that the degassing is exactly at its limit between diluted and non-diluted, giving bubble cluster diameters of 3.5–4.6 mm and 3.8–8.2 mm, for underlying gas fluxes of 0.52 m^3/s and 0.80 m^3/s, respectively, as prior to the Subplinian phase. I have also proposed and quantified a new degassing process in a magma reservoir, that resulting from bubble clusters. The early formation of the bubble clusters, by hindering the bubble growth by gas diffusion after their nucleation, can explain the very small bubble diameter at Shishaldin.

The degassing parameters in magma reservoir, such as bubble diameter, underlying gas flux, gas volume fraction, radius of the reservoir, have shown that the specificity of the Subplinian activity at Shishaldin lies in having simultaneously the smallest bubble diameter with the largest underlying gas flux, when compared with Etna, the Kilauea Iki eruption Kīlauea and Erta 'Ale. The diagram of the underlying gas flux as a function of bubble diameter for these four volcanoes had also shown that Etna, during its high-level lava fountaining activity, is the closest to the Subplinian regime, when compared to Kīlauea and Erta 'Ale, as expected due to the 1.8% occurrence of Subplinian basaltic eruptions at Etna (Coltelli et al., 1995, 2000). This diagram also shows how contrasted are the underlying gas flux and bubble diameter between Shishaldin and Erta 'Ale despite being both produced by a quasi-stable foam in the reservoir and a similar reservoir radius. This study gives the basis for drawing a diagram regime for all basaltic eruptive types. Lastly, the differences in degassing parameters between these four volcanoes are associated to a difference in the magma ascent rate, very large at Shishaldin, large for the Kilauea Iki eruption at Kīlauea, intermediate at Etna and small at Erta 'Ale.

The interpretation of the Shishaldin eruption, by being consistent in both its degassing parameters in the reservoir when compared to other basaltic volcanoes and its reservoir size, small, as deduced from the lack of deformations (Moran et al., 2006), suggest that our foam model is very robust. Indeed this model only requires two conditions, first having exsolved gas in the reservoir, as shown to be the case (Rasmussen et al., 2018; Stelling et al., 2002), and second a moderate change in radius between the reservoir and the conduit, largely met by a factor $\geq$30 at Shishaldin, whereas a factor of $\geq$6 is largely sufficient. The behavior of the foam at the top of magma reservoir can now explain the four main regimes of basaltic activity, such as the weak and typical Strombolian activity, the high-level lava fountains, and the Subplinian eruptive column simply by changing the underlying gas flux and the bubble diameter in the magma reservoir.

Appendix A: Errors on Gas Volumes During Eruptive Columns

Our estimates on the gas volumes have been deduced from infrasound measurements done with a single sensor, either for the typical or weak Strombolian explosions or for eruptive columns, such as for the Subplinian column or the two thermals occurring in the middle of the pre-Subplinian phase (Figure 1). The source of sound for the Strombolian explosions have been previously associated to a monopole, that is, a source characterized by a time-varying mass flux and radiating (hemi)-spherically within the atmosphere (Vergniolle & Caplan-Auerbach, 2004; Vergniolle et al., 2004), the measurements of the radiation pattern showing that this assumption is mostly valid roughly within a $\pm$10% error at Erebus (Gerst et al., 2013; Johnson et al., 2008), Yasur (Jolly et al., 2017) and Sakurajima (Fee et al., 2017). Vulcanian explosions at Tungurahae were best modeled as a dipole, that is, a pair of acoustic monopoles with opposite sign imparting a net force on the fluid (Kim et al., 2012). The gas volume emitted by the Subplinian column and the two thermals was deduced from the vent radius and the temporal evolution of the gas velocity (Vergniolle & Caplan-Auerbach, 2006).

Power laws have been proposed to relate the gas velocity to the infrasonic power, with different empirical coefficients depending on the type of source, monopole, dipole or quadrupole, that is, formed by two dipoles (Woulff & MacGetchin, 1976). We had assumed that the radiation of sound during an eruptive column is that of a dipole, and that infrasonic power is related to the power 6 of the gas velocity (Vergniolle & Caplan-Auerbach, 2006). This simple power law was validated for eruptive columns, such as at Mt Augustine (Alaska) by comparing with plume heights (Caplan-Auerbach et al., 2010) and at Eyjafjallajökull (Iceland) by comparing with thermal videos (Ripepe et al., 2013). Hence the gas velocity during the Subplinian column, found to be 82 $\pm$ 3.2 m/s (Vergniolle & Caplan-Auerbach, 2006), is probably a reasonable estimate.

However a proper estimate of the gas velocity should take into account the directionality of the infrasonic source (Matoza et al., 2013), previously assumed to be a dipole radiating in a hemisphere (Vergniolle & Caplan-Auerbach, 2006). Furthermore the intensity, which depends on the angle between sensor and the axis of the eruptive column, should be used rather than infrasonic power (Matoza et al., 2013). Scaling laws relating gas velocity to the infrasonic intensity have been proposed and tested for conditions very different from the eruptive columns, which are hot multiphase flows (Matoza et al., 2013; Tam, 2019; Tam et al., 2008). These scaling laws depends on (a) two empirical coefficients, which are totally unknown for volcanic conditions, (b) the temperature ratio between that of the volcanic mixture and that of the atmosphere and (c) the Mach number, that is, the ratio between the velocity of the volcanic dusty gas and the sound speed. The source of the sound of a jet have been associated to both fine-scale turbulence and large-scale turbulence, each of these sources having a different angle of emission (Tam, 2019; Tam et al., 2008). Self-similarity spectra have been proposed for these two sources based on a few reference set-ups, such as supersonic flows at laboratory scale, military aircrafts or rocket motors (Tam, 2019; Tam et al., 2008).

The jet noise produced by a Plinian eruptive column at Shinmoe-dake (Japan), however, does not agree with the above jet noise models and cannot explain the infrasonic eruptive tremor and the seismic eruptive tremor (Ichihara, 2016). In contrast, the spectra produced by a phreatic eruption at Mount St Helens (USA) and heavily particle-laden flows at Tungurahae (Ecuador), both of which being classified between Vulcanian and Plinian, mostly falls into the regime whose sound is dominated by large-scale turbulence, despite a significant mismatch at mid-frequency (Matoza et al., 2009). This result is remarkable because the operating conditions of eruptive columns are very far from the database used to validate the self-similarity solutions (Matoza et al., 2009; Tam, 2019). The potential errors made in using the infrasonic power with the assumption of isotropic spherical radiation (Vergniolle & Caplan-Auerbach, 2006) have been estimated using the above database (Matoza

et al., 2013). Previous estimates of the gas velocity may have to be multiplied by a factor 1.2 to 1.6, depending on experimental reference set-ups used to calibrate errors, giving 135 m/s as the maximum estimate of the average gas velocity at Shishaldin. The wide range of values potentially applicable to volcanoes added to the other uncertainties associated to the source of the sound, with the drastically different operating conditions than those corresponding to the analog jets noise (Matoza et al., 2013), have prevented me to use these scaling laws for the Subplinian column or the two thermals produced by Shishaldin volcano. Therefore the average gas velocity during the Subplinian column is likely to be between 82 m/s (Vergniolle & Caplan-Auerbach, 2006) and 135 m/s. However the temporal evolution of the gas velocity was probably correctly estimated by previous studies (Vergniolle & Caplan-Auerbach, 2006) because the conditions within the volcanic jet are unlikely to change dramatically within the different periods of the Subplinian eruptive column or that of the two thermals. Hence the total gas volumes emitted during the Subplinian columns and the two thermals only need to be rescaled by the range of values possible for the average gas velocity.

Gas velocities were found to be 93–220 m/s for the Vulcanian blasts at Mt Augustine (Caplan-Auerbach et al., 2010) and 54–142 m/s for the 4–8 km eruptive columns at Eyjafjallajökull (Ripepe et al., 2013). Muzzle velocities of 150 m/s and 170 m/s were estimated for the two Plinian eruptions of Masaya (Nicaragua) (Williams, 1983) and up to 250 m/s for the 1886 Tarawera eruption (Walker et al., 1984). Vulcanian explosions at Soufrière Hills (Montserrat Island, West Indies) was also estimated between 40 m/s and 180 m/s (Druitt et al., 2002). It is important to note that the Subplinian column or the two thermals do not start with initial decompression, unlike Vulcanian explosions or large Plinian column. We therefore expect the gas velocity at Shishaldin to be below the above values. Our maximum estimate of the average gas velocity, 135 m/s, which is comparable with other values found for similar eruptive patterns, is probably an upper limit due to the lack of initial decompression.

Data Availability Statement

All the necessary informations to reproduce all the results presented in this paper can be found in Vergniolle (2024a, 2024b). The model for predicting magma viscosity can be found in Giordano et al. (2008a, 2008b) and the calculations of the reduced displacement in Thompson (2023).

Acknowledgments
I am grateful for the support of the AVO and mostly to Jackie Caplan-Auerbach for her thoughts, time and help. I'm also grateful to Glenn Thompson, who has provided an open access link for his calculations of seismic reduced displacement. I also thank M. Mangan, L. Mastin, J Larsen, M. Colombier, D. Baker and two anonymous reviewer for very careful reviews, C. Le Losq, N. Métrich, M. Pichavant, D. Laporte and Y. Gaudemer for their help and D. Schmitt for his detailed editorial work. This work was supported by an internal funding from Institut de Physique du Globe de Paris (BQR, 2018) and the Tellus Program of CNRS/INSU (2020) for understanding basaltic eruptive columns.

References

Albarède, F. (1993). Residence time analysis of geochemical fluctuations in volcanic series. *Geochimica et Cosmochimica Acta*, *57*(3), 615–621. https://doi.org/10.1016/0016-7037(93)90372-4

Alfano, F., Ort, M. H., Pioli, L., Self, S., Hanson, S. L., Roggensack, K., et al. (2018). Subplinian monogenetic basaltic eruption of Sunset Crater, Arizona, USA. *GSA Bulletin*, *131*(3–4), 661–674. https://doi.org/10.1130/b31905.1

Allard, P., Burton, M., & Muré, F. (2005). Spectroscopic evidence for a lava fountain driven by previously accumulated magmatic gas. *Nature*, *433*(7024), 407–410. https://doi.org/10.1038/nature03246

Allison, C., Roggensack, K., & Clarke, A. B. (2021). Highly explosive basaltic eruptions driven by CO_2 exsolution. *Nature Communications*, *12*(1), 217. https://doi.org/10.1038/s41467-020-20354-2

Arzilli, F. M., Polacci, G., La Spina, N., Le Gall, E. W., Llewellin, R. A., Brooker, M. E., et al. (2022). Dendritic crystallization in hydrous basaltic magmas controls magma mobility within the Earth's crust. *Nature Communication*, *13*, 3354. https://doi.org/10.1038/s41467-022-30890-8

Bai, L., Baker, D. R., & Rivers, M. (2008). Experimental study of bubble growth in Stromboli basalt melts at 1 atm. *Earth and Planetary Science Letters*, *267*(3–4), 533–547. https://doi.org/10.1016/j.epsl.2007.11.063

Bamber, E. C., Arzilli, F., Polacci, M., Hartley, M. E., Fellowes, J., Di Genova, D., et al. (2020). Pre- and syn-eruptive conditions of a basaltic Plinian eruption at Masaya volcano, Nicaragua: The Masaya Triple Layer (2.1 ka). *Journal of Volcanology and Geothermal Research*, *392*, 106761. https://doi.org/10.1016/j.jvolgeores.2019.106761

Bamber, E. C., La Spina, G., Arzilli, F., de Michieli Vitturi, M., Polacci, M., Hartley, M. E., et al. (2022). Basaltic Plinian eruptions at Las Sierras-Masaya volcano driven by cool storage of crystal-rich magmas. *Communications Earth & Environment*, *3*(1), 253. https://doi.org/10.1038/s43247-022-00585-5

Barclay, J., Riley, D. S., & Sparks, R. S. J. (1995). Analytical models for bubble growth during decompression of high viscosity magma. *Bulletin of Volcanology*, *57*(6), 422–431. https://doi.org/10.1007/s004450050102

Beget, J., Nye, C., & Stelling, P. (1998). Postglacial collapse and regrowth of Shishaldin volcano, Alaska, based on historic and prehistoric tephrochronology. *Eos Trans Am Geophys Union*, *79*, F979.

Beget, J. E., Nye, C. J., Schaefer, J. R., & Stelling, P. (2003). Preliminary volcano-hazard assessment for Shishaldin volcano, Alaska, Alaska Department of Natural ressources. Report of investigation 2002-4.

Bottinga, Y., & Javoy, M. (1989). MORB degassing: Evolution of CO_2. *Earth and Planetary Science Letters*, *95*(3–4), 215–225. https://doi.org/10.1016/0012-821x(89)90098-8

Bottinga, Y., & Javoy, M. (1990). MORB degassing: Bubble growth and ascent. *Chemical Geology*, *81*(4), 255–270. https://doi.org/10.1016/0009-2541(90)90050-h

Brennen, C. E. (1995). Cavitation and bubble dynamics. In *Oxford engineering science series* (Vol. 44, p. 282). Oxford University Press.

Brennen, C. E. (2005). *Fundamental of multiphase flow* (p. 345). Cambridge University Press.

Burton, M., Allard, P., Murè, F., & La Spina, A. (2007). Magmatic gas composition reveals the source depth of slug-driven strombolian explosive activity. *Science*, *317*(5835), 227–230. https://doi.org/10.1126/science.1141900

Calvari, S., & Research Staff of the Instituto Nazionale di Geofisica e Vulcanologia- Sezione di Catania, Italy. (2001). *Eos Trans Am Geophys Union*, *82*(52), 653–656.

Cantat, I., Cohen-Addad, S., Elias, F., Graner, F., Höhler, R., Pitois, O., et al. (2013). *Foams, structure and dynamics*. Oxford University Press.

Caplan-Auerbach, J., Bellesiles, A., & Fernandes, J. K. (2010). Estimates of eruption velocity and plume height from infrasonic recordings of the 2006 eruption of Augustine volcano, Alaska. *Journal of Volcanology and Geothermal Research*, *189*(1–2), 12–18. https://doi.org/10.1016/j.jvolgeores.2009.10.002

Caplan-Auerbach, J., & McNutt, S. R. (2003). New insights into the 1999 eruption of Shishaldin volcano based on acoustic data. *Bulletin of Volcanology*, *65*(6), 405–417. https://doi.org/10.1007/s00445-002-0267-5

Caplan-Auerbach, J., & Petersen, T. (2005). Repeating coupled earthquakes at Shishaldin volcano, Alaska. *Journal of Volcanology and Geothermal Research*, *145*(1–2), 151–172. https://doi.org/10.1016/j.jvolgeores.2005.01.011

Carey, R. J., Houghton, B. F., Sable, J. E., & Wilson, C. J. N. (2007). Contrasting grain size and componentry in complex proximal deposits of the 1886 Tarawera basaltic plinian eruption. *Bulletin of Volcanology*, *69*(8), 903–926. https://doi.org/10.1007/s00445-007-0117-6

Cashman, K. V., & Mangan, M. T. (1994). Physical aspects of magma degassing II, Constraints on vesiculation processes from textural studies of eruptive products. In M. R. Carroll & J. R. Holloway (Eds.), *Volatiles in magmas* (pp. 446–478). Mineralogical Society of America.

Castro, J. M., Burgisser, A., Schipper, C. I., & Mancini, S. (2012). Mechanisms of bubble coalescence in silicic magmas. *Bulletin of Volcanology*, *74*(10), 2339–2352. https://doi.org/10.1007/s00445-012-0666-1

Chavrit, D., Humler, E., Morizet, Y., & Laporte, D. (2012). Influence of magma ascent rate on carbon dioxide degassing at oceanic ridges: Message in a bubble. *Earth and Planetary Science Letters*, *357–358*, 376–385. https://doi.org/10.1016/j.epsl.2012.09.042

Coltelli, M., Del Carlo, P., & Vezzoli, L. (1995). Stratigraphy of the holocene Mt. Etna explosion eruptions. *Periodico di Mineralogia*, *64*, 141–143.

Coltelli, M., Del Carlo, P., & Vezzoli, L. (1998). Discovery of a Plinian basaltic eruption of Roman age at Etna volcano, Italy. *Geology*, *26*(12), 1095–1098. https://doi.org/10.1130/0091-7613(1998)026<1095:doapbe>2.3.co;2

Coltelli, M., Del Carlo, P., & Vezzoli, L. (2000). Stratigraphic constraints for explosive activity in the past 100 ka at Etna volcano, Italy. *International Journal of Earth Sciences*, *89*(3), 665–677. https://doi.org/10.1007/s005310000117

Condomines, M., Tanguy, J.-C., & Michaud, V. (1995). Magma dynamics at Mt Etna: Constraints from U-Th-Ra-Pb radioactive disequilibria and Sr isotopes in historical lavas. *Earth and Planetary Science Letters*, *132*(1–4), 25–41. https://doi.org/10.1016/0012-821x(95)00052-e

Cusano, P., Palo, M., & West, M. E. (2015). Long-period seismicity at Shishaldin volcano (Alaska) in 2003–2004: Indications of an upward migration of the source before a minor eruption. *Journal of Volcanology and Geothermal Research*, *291*, 14–24. https://doi.org/10.1016/j.jvolgeores.2014.12.008

Del Bello, E., Llewellin, E. W., Taddeucci, J., Scarlato, P., & Lane, S. (2012). An analytical model for gas overpressure in slug-driven explosions: Insights into Strombolian volcanic eruptions. *Journal of Geophysical Research: Solid Earth*, *117*, B02206. https://doi.org/10.1029/2011JB008747

Druitt, T. H., Young, S. R., Baptie, B., Bonadonna, C., Calder, E. S., Clarke, A. B., et al. (2002). Episodes of cyclic Vulcanian explosive activity with fountain collapse at Soufrière Hills Volcano, Montserrat. In T. H. Druitt & B. P. Kokelaar (Eds.), *The eruptions of Soufrière Hills volcano, Montserrat, from 1995 to 1999* (Vol. 21, pp. 281–306). Geological Society.

Edmonds, M., & Gerlach, T. M. (2007). Vapor segregation and loss in basaltic melts. *Geology*, *35*(8), 751–754. https://doi.org/10.1130/g23464a.1

Edmonds, M., Sides, I. R., Swanson, D. A., Werner, C., Martin, R. S., Mather, T. A., et al. (2013). Magma storage, transport and degassing during the 2008-10 summit eruption at Kīlauea Volcano, Hawai'i. *Geochimica et Cosmochimica Acta*, *123*, 284–301. https://doi.org/10.1016/j.gca.2013.05.038

Fee, D., Izbekov, P., Kim, K., Yokoo, A., Lopez, T., Prata, F., et al. (2017). Eruption mass estimation using infrasound waveform inversion and ash and gas measurements: Evaluation at Sakurajima Volcano, Japan. *Earth and Planetary Science Letters*, *480*, 42–52. https://doi.org/10.1016/j.epsl.2017.09.043

Fee, D., Toney, L., Kim, K., Sanderson, R. W., Iezzi, A. M., Matoza, R. S., et al. (2021). Local explosion detection and infrasound localization by reverse time migration using 3-D finite-difference wave propagation. *Frontiers in Earth Science*, *9*, 620813. https://doi.org/10.3389/feart.2021.620813

Ferguson, D., Gonnermann, H. M., Ruprecht, P., Plank, T., Hauri, E. H., Houghton, B. F., & Swanson, D. A. (2016). Magma decompression rates during explosive eruptions of Kīlauea Volcano, Hawai'i, recorded by melt embayments. *Bulletin of Volcanology*, *78*(10), 71. https://doi.org/10.1007/s00445-016-1064-x

Fiske, R. S., Rose, T. R., Swanson, D. A., & McGeehin, J. C. (1999). The Kulanaokuaiki tephra: Product of newly recognised pyroclastic eruptions at Kīlauea volcano, Hawai'i. *Eos Trans Am Geophys Union*, *80*(46), 1196–1197.

Fiske, R. S., Rose, T. R., Swanson, D. A., & McGeehin, J. C. (2000). Kulanaokuaiki 3 tephra: Produce of an energetic pyroclastic eruption at Kīlauea volcano, Hawai'i. *Eos Trans Am Geophys Union*, *81*(47), V11B–V13.

Gardner, J. E., & Denis, M. H. (2004). Heterogeneous bubble nucleation on Fe-Ti oxide crystals in high-silica rhyolitic melts. *Geochimica et Cosmochimica Acta*, *68*(17), 3587–3597. https://doi.org/10.1016/j.gca.2004.02.021

Gardner, J. E., Ketcham, R. A., & Moore, G. (2013). Surface tension of hydrous silicate melts: Constraints on the impact of melt composition. *Journal of Volcanology and Geothermal Research*, *267*, 68–74. https://doi.org/10.1016/j.jvolgeores.2013.09.007

Gardner, J. E., Thomas, R. M. E., Jaupart, C., & Tait, S. (1996). Fragmentation of magma during Plinian volcanic eruptions. *Bulletin of Volcanology*, *58*(2–3), 144–162. https://doi.org/10.1007/s004450050132

Gerst, A., Hort, M., Aster, R., Johnson, J. B., & Kyle, P. R. (2013). The first second of volcanic eruptions from the Erebus volcano lava lake, Antarctica–Energies, pressures, seismology, and infrasound. *Journal of Geophysical Research: Solid Earth*, *118*(7), 3318–3340. https://doi.org/10.1002/jgrb.50234

Giordano, D., & Dingwell, D. B. (2003). Viscosity of hydrous Etna basalt: Implications for Plinian-style basaltic eruptions. *Bulletin of Volcanology*, *65*(1), 8–14. https://doi.org/10.1007/s00445-002-0233-2

Giordano, D., Russell, J. K., & Dingwell, D. B. (2008a). Viscosity of magmatic liquids: A model. *Earth and Planetary Science Letters*, *271*(1–4), 123–134. https://doi.org/10.1016/j.epsl.2008.03.038

Giordano, D., Russell, J. K., & Dingwell, D. B. (2008b). Model for predicting the viscosity of magmatic liquids: A model (version v1.0.1) [Software written in Excel and Matlab]. https://www.eoas.ubc.ca/krussell/VISCOSITY/grdViscosity.html

Goepfert, K., & Gardner, J. E. (2010). Influence of pre-eruptive storage conditions and volatile contents on explosive Plinian style eruptions of basic magma. *Bulletin of Volcanology*, *72*, 511–521. https://doi.org/10.1007/s00445-010-0343-1

Gresta, S., Ripepe, M., Marchetti, E., D'Amico, S., Coltelli, M., Harris, A. J. L., & Privitera, E. (2004). Seismo-acoustic measurements during July-August 2001 eruption of Mt Etna volcano, Italy. *Journal of Volcanology and Geothermal Research*, *137*(1–3), 219–230. https://doi.org/10.1016/j.jvolgeores.2004.05.017

Hamada, M., Laporte, D., Cluzel, N., Koga, K. T., & Kawamoto, T. (2010). Simulating bubble number density of rhyolitic pumices from Plinian eruptions: Constraints from fast decompression experiments. *Bulletin of Volcanology*, *72*(6), 735–746. https://doi.org/10.1007/s00445-010-0353-z

Happel, J., & Brenner, H. (1973). *Mechanics of fluids and transport processes: Low Reynolds number hydrodynamics* (p. 553). Kluwer Academic Publishers.

Houghton, B. F., & Gonnermann, H. M. (2008). Basaltic explosive volcanism: Constraints from deposits and models. *Geochemistry*, *68*(2), 117–140. https://doi.org/10.1016/j.chemer.2008.04.002

Houghton, B. F., Wilson, C. J. N., Del Carlo, P., Coltelli, M., Sable, J. E., & Carey, R. (2004). The influence of conduit processes on changes in style of basaltic Plinian eruptions: Tarawera 1986 and Etna 122 BC. *Journal of Volcanology and Geothermal Research*, *137*(1–3), 1–14. https://doi.org/10.1016/j.jvolgeores.2004.05.009

Ichihara, M. (2016). Seismic and infrasonic eruption tremors and their relation to magma discharge rate: A case study for sub-Plinian events in the 2011 eruption of Shinmoe-dake, Japan. *Journal of Geophysical Research: Solid Earth*, *121*(10), 7101–7118. https://doi.org/10.1002/2016JB013246

Ikenaga, Y., Maeno, F., & Yasuda, A. (2023). Temporal change in eruption style during the basaltic explosive An'ei eruption of the Izu-Oshima volcano, Japan: Insights from stratigraphy and chemical composition analyses. *Frontiers in Earth Science*, *11*, 1172615. https://doi.org/10.3389/feart.2023.1172615

Jaupart, C., & Allègre, C. J. (1991). Gas content, eruption rate and instabilities of eruption regime in silicic volcanoes. *Earth and Planetary Science Letters*, *102*(3–4), 413–429. https://doi.org/10.1016/0012-821x(91)90032-d

Jaupart, C., & Vergniolle, S. (1988). Laboratory models of Hawaiian and Strombolian eruptions. *Nature*, *331*(6151), 58–60. https://doi.org/10.1038/331058a0

Jaupart, C., & Vergniolle, S. (1989). The generation and collapse of a foam layer at the roof of a basaltic magma chamber. *Journal of Fluid Mechanics*, *203*, 347–380. https://doi.org/10.1017/s0022112089001497

Johnson, J. B., Aster, R. C., Kyle, P. R., McIntosh, W., & McIntosh, B. (2008). Acoustic source characterization of impulsive Strombolian eruptions from the Mount Erebus lava lake. *Journal of Volcanology and Geothermal Research*, *177*(3), 673–686. https://doi.org/10.1016/j.jvolgeores.2008.06.028

Jolly, A. D., Matoza, R. S., Fee, D., Kennedy, B. M., Iezzi, A. M., Fitzgerald, R. H., et al. (2017). Capturing the acoustic radiation pattern of strombolian eruptions using infrasound sensors aboard a Tethered Aerostat, Yasur volcano, Vanuatu. *Geophysical Research Letters*, *44*(19), 9672–9680. https://doi.org/10.1002/2017GL074971

Khitarov, N. I., Lebedev, Y. B., Dorfman, A. M., & Bagdasarov, N. S. (1979). Effects of temperature, pressure, and volatiles on the surface tension of molten basalt. *Geochemistry International*, *16*(5), 78–86.

Kim, K., Lees, J. M., & Ruiz, M. (2012). Acoustic multipole source model for volcanic explosions and inversion for source parameters. *Geophysical Journal International*, *191*(3), 1192–1204. https://doi.org/10.1111/j.1365-246x.2012.05696.x

Larsen, J. F. (2016). Unraveling the diversity in arc volcanic eruption styles: Examples from the Aleutian volcanic arc, Alaska. *Journal of Volcanology and Geothermal Research*, *327*, 643–668. https://doi.org/10.1016/j.jvolgeores.2016.09.008

La Spina, A., Burton, M., Allard, P., Alparone, S., & Muré, F. (2015). Open-path FTIR spectroscopy of magma degassing processes during eight lava fountains on Mount Etna. *Earth and Planetary Science Letters*, *413*, 123–134. https://doi.org/10.1016/j.epsl.2014.12.038

La Spina, G., Arzilli, F., Llewellin, E. W., Burton, M. R., Clarke, A. B., Vitturi, M. D. M., et al. (2021). Explosivity of basaltic lava fountains is controlled by magma rheology, ascent rate and outgassing. *Earth and Planetary Science Letters*, *553*, 116658. https://doi.org/10.1016/j.epsl.2020.116658

Le Cloarec, M. F., & Pennisi, M. (2001). Radionucleides and sulfur content in mount Etna plume in 1983-1995: New constraints on the magma feeding system. *Journal of Volcanology and Geothermal Research*, *108*(1–4), 141–155. https://doi.org/10.1016/s0377-0273(00)00282-1

Le Gall, N., & Pichavant, M. (2016a). Experimental simulation of bubble nucleation and magma ascent in basaltic systems: Implications for Stromboli volcano. *American Mineralogist*, *101*(9), 1967–1985. https://doi.org/10.2138/am-2016-5639

Le Gall, N., & Pichavant, M. (2016b). Homogeneous bubble nucleation in H_2O- and H_2O-CO_2-bearing basaltic melts: Results of high temperature decompression experiments. *Journal of Volcanology and Geothermal Research*, *327*, 604–621. https://doi.org/10.1016/j.jvolgeores.2016.10.004

Lensky, N. G., Navon, O., & Lyakhovsky, V. (2004). Bubble growth during decompression of magma: Experimental and theoretical investigation. *Journal of Volcanology and Geothermal Research*, *129*(1–3), 7–22. https://doi.org/10.1016/s0377-0273(03)00229-4

Lloyd, A. S., Ruprecht, P., Hauri, E. H., Rose, W., Gonnermann, H. M., & Plank, T. (2014). NanoSIMS results from olivine-hosted melt embayments: Magma ascent rate during explosive basaltic eruptions. *Journal of Volcanology and Geothermal Research*, *283*, 1–18. https://doi.org/10.1016/j.jvolgeores.2014.06.002

Lu, Z., & Dzurisin, D. (2014). *InSAR imaging of Aleutian volcanoes, monitoring a volcanic arc from space* (p. 388). Springer. https://doi.org/10.1007/978-3-642-00348-6

Lu, Z., Dzurisin, D., Wicks, C., Jr., Power, J., Kwoun, O., & Rykhus, R. (2007). Diverse deformation patterns of Aleutian volcanoes from satellite interferometric synthetic aperture radar (InSAR). In *Volcanism and subduction: The Kamchatka region* (Vol. 172, pp. 249–261). Geophysical Monograph Series. https://doi.org/10.1029/172gm18

Lu, Z., Wicks, C., Dzurisin, D., Power, J., Thatcher, W., & Masterlark, T. (2003). Interferometric synthetic aperture radar studies of Alaska volcanoes. *Earth Observation Magazine*, *12*(3).

Lyakhovsky, W., Hurwitz, S., & Navon, O. (1996). Bubble growth in rhyolitic melts: Experimental and numerical investigation. *Bulletin of Volcanology*, *58*(1), 19–32. https://doi.org/10.1007/s004450050122

Mader, H. M., Llewellin, E. W., & Mueller, S. P. (2013). The rheology of two-phase magmas: A review and analysis. *Journal of Volcanology and Geothermal Research*, *257*, 135–158. https://doi.org/10.1016/j.jvolgeores.2013.02.014

Manga, M., & Stone, H. A. (1995). Collective hydrodynamics of deformable drops and bubbles in dilute low Reynolds number suspensions. *Journal of Fluid Mechanics*, *300*, 231–263. https://doi.org/10.1017/s0022112095003673

Mangan, M. T., & Cashman, K. V. (1996). The structure of basaltic scoria and reticulite and inferences for vesiculation, foam formation, and fragmentation in lava fountains. *Journal of Volcanology and Geothermal Research*, *73*(1–2), 1–18. https://doi.org/10.1016/0377-0273(96)00018-2

Mangan, M. T., & Sisson, T. (2005). Evolution of melt-vapor surface tension in silicic volcanic systems: Experiments with hydrous melts. *Journal of Geophysical Research*, *110*(B01202), 1–9. https://doi.org/10.1029/2004jb003215

Massey, B. S. (1989). *Mechanics of fluid* (p. 599). Chapman and Hall.
Matoza, R. S., Fee, D., Garcés, M. A., Seiner, J. M., Ramón, P. A., & Hedlin, M. A. H. (2009). Infrasonic jet noise from volcanic eruptions. *Geophysical Research Letters*, *36*(8), L08303. https://doi.org/10.1029/2008GL036486
Matoza, R. S., Fee, D., Neilsen, T. B., Gee, K. L., & Ogden, D. E. (2013). Aeroacoustics of volcanic jets: Acoustic power estimation and jet velocity dependence. *Journal of Geophysical Research: Solid Earth*, *118*(12), 6269–6284. https://doi.org/10.1002/2013JB010303
Métrich, N., Allard, P., Spilliaert, N., Andronico, D., & Burton, M. (2004). 2001 flank eruption of the alkali-and volatile-rich primitive basalt responsible for Mount Etna's evolution in the last three decades. *Earth and Planetary Science Letters*, *228*(1–2), 1–17. https://doi.org/10.1016/j.epsl.2004.09.036
Moitra, P., Gonnermann, H. M., Houghton, B. F., & Tiwary, C. S. (2018). Fragmentation and Plinian eruption of crystallizing basaltic magma. *Earth and Planetary Science Letters*, *500*, 97–104. https://doi.org/10.1016/j.epsl.2018.08.003
Moore, J. G. (1965). Petrology of deep-sea basalt near Hawai'i. *American Journal of Science*, *263*(1), 40–52. https://doi.org/10.2475/ajs.263.1.40
Moretti, R., Métrich, N., Arienzo, I., Di Renzo, V., Aiuppa, A., & Allard, P. (2018). Degassing vs. eruptive styles at Mt. Etna volcano (Sicily, Italy). Part I: Volatile stocking, gas fluxing, and the shift from low-energy to highly explosive basaltic eruptions. *Chemical Geology*, *482*, 1–17. https://doi.org/10.1016/j.chemgeo.2017.09.017
Mourtada-Bonnefoi, C. C., & Laporte, D. (2002). Homogeneous bubble nucleation in rhyolitic magmas: An experimental study of the effect of H_2O and CO_2. *Journal of Geophysical Research*, *107*(B4), 1–19. https://doi.org/10.1029/2001JB000290
Mourtada-Bonnefoi, C.C., & Laporte, D. (2004). Kinetics of bubble nucleation in a rhyolitic melt: An experimental study of the effect of ascent rate. *Earth and Planetary Science Letters*, *218*, 521–537.
Moran, S. C., Kwoun, O., Masterlark, T., & Lu, Z. (2006). On the absence of InSAR-detected volcano deformation spanning the 1995–1996 and 1999 eruptions of Shishaldin volcano, Alaska. *Journal of Volcanology and Geothermal Research*, *150*, 19–31.
Namiki, A., & Manga, M. (2006). Influence of decompression rate on the expansion velocity and expansion style of bubbly fluids. *Journal of Geophysical Research*, *111*(B11), B11208. https://doi.org/10.1029/2005JB004132
Navon, O., & Lyakhovsky, V. (1998). Vesiculation processes in silicic magmas, the physics of explosive volcanic eruptions. In J. S. Gilbert & R. S. J. Sparks (Eds.) (Vol. *145*, pp. 27–50). Geological Society Special Publicaion.
Neethling, S. J., Lee, H. T., & Grassia, P. (2005). The growth, drainage and breakdown of foam. *Colloids and Surface A: Physicochem. Eng. Aspects*, *263*(1–3), 184–196. https://doi.org/10.1016/j.colsurfa.2004.12.014
Nye, C. J., Keith, T., Eichelberger, J. C., Miller, T. P., McNutt, S. R., Moran, S. C., et al. (2002). The 1999 eruption of Shishaldin volcano, Alaska: Monitoring a distant eruption. *Bulletin of Volcanology*, *64*(8), 507–519. https://doi.org/10.1007/s00445-002-0225-2
Parfitt, E. A. (2004). A discussion of the mechanisms of explosive basaltic eruptions. *Journal of Volcanology and Geothermal Research*, *134*(1–2), 77–107. https://doi.org/10.1016/j.jvolgeores.2004.01.002
Parfitt, E. A., Wilson, L., & Neal, C. A. (1995). Neal, factors influencing the height of Hawaiian lava fountains: Implications for the use of fountain height as an indicator of magma content. *Bulletin of Volcanology*, *57*, 440–450.
Parfitt, E. A., & Wilson, L. (1995). Explosive volcanic eruptions: IX the transition between Hawaiian-style lava fountaining and strombolian explosive activity. *Geophysical Journal International*, *121*(1), 226–232. https://doi.org/10.1111/j.1365-246x.1995.tb03523.x
Petersen, T., De Angelis, S., Tytgat, G., & McNutt, S. R. (2006). Local infrasound observations of large ash explosions at Augustine Volcano, Alaska, during January 11-28, 2006. *Geophysical Research Letters*, *33*, L12303. https://doi.org/10.1029/2006GL026491
Petersen, T., & McNutt, S. R. (2007). Seismo-acoustic signals associated with degassing explosions recorded at Shishaldin volcano, Alaska, 2003-2004. *Bulletin of Volcanology*, *69*(5), 527–536. https://doi.org/10.1007/s00445-006-0088-z
Pichavant, M., Di Carlo, I., Pompilio, M., & Le Gall, N. (2022). Timescales and mechanisms of paroxysm initiation at Stromboli volcano, Aeolian Islands, Italy. *Bulletin of Volcanology*, *84*(36), 36. https://doi.org/10.1007/s00445-022-01545-9
Pichavant, M., Di Carlo, I., Rotolo, S. G., Scaillet, B., Burgisser, A., Le Gall, N., & Martel, C. (2013). Generation of CO_2-rich melts during basalt magma ascent and degassing. *Contributions to Mineralogy and Petrology*, *166*(2), 545–561. https://doi.org/10.1007/s00410-013-0890-5
Polacci, D. R. B., Bai, L., & Mancini, L. (2008). Large vesicles record pathways of degassing at basaltic volcanoes. *Bulletin of Volcanology*, *70*(9), 1023–1029. https://doi.org/10.1007/s00445-007-0184-8
Polacci, M., Baker, D. R., LaRue, A., Mancini, L., & Allard, P. (2012). Degassing behaviour of vesiculated basaltic magmas: An example from Ambrym volcano, Vanuatu arc, and comparison to Stromboli, Aeolian Islands, Italy. *Journal of Volcanology and Geothermal Research*, *233–234*, 55–64. https://doi.org/10.1016/j.jvolgeores.2012.04.019
Polacci, M., Baker, D. R., Mancini, L., Tromba, G., & Zanini, F. (2006). Three-dimensional investigation of volcanic textures by X-ray microtomography and implications for conduit processes. *Geophysical Research Letters*, *33*(13), L13312. https://doi.org/10.1029/2006GL026241
Proussevitch, A. A., & Kutolin, V. A. (1986). Surface tension of magmatic melts (in Russian). *Geological Geophysics*, *9*, 58–67.
Proussevitch, A. A., & Sahagian, D. L. (1996). Dynamics of coupled diffusive and decompressive bubble growth in magmatic systems. *Journal of Geophysical Research*, *101*(B8), 17447–17455. https://doi.org/10.1029/96jb01342
Proussevitch, A. A., & Sahagian, D. L. (1998). Dynamics and energetics of bubble growth in magmas: Analytical formulation and numerical modeling. *Journal of Geophysical Research*, *103*(B8), 18223–18251. https://doi.org/10.1029/98jb00906
Proussevitch, A. A., Sahagian, D. L., & Kutolin, V. A. (1993). Stability of foams in silicate melts. *Journal of Volcanology and Geothermal Research*, *59*(1–2), 161–178. https://doi.org/10.1016/0377-0273(93)90084-5
Prud'homme, R. K., & Khan, S. A. (1996). *Foams: Theory, measurements, and applications* (p. 590). Marcel Dekker Inc.
Rasmussen, D. J., Plank, T. A., Roman, D. C., Power, J. A., Bodnar, R. J., & Hauri, E. H. (2018). When does eruption run-up begin? Multi-disciplinary insight from the 1999 eruption of Shishaldin volcano. *Earth and Planetary Science Letters*, *486*, 1–14. https://doi.org/10.1016/j.epsl.2018.01.001
Ripepe, M., Bonadonna, C., Folch, A., Delle Donne, D., Lacanna, G., Marchetti, E., & Höskuldsson, A. (2013). Ash-plume dynamics and eruption source parameters by infrasound and thermal imagery: The 2010 Eyjafjallajökull eruption. *Earth and Planetary Science Letters*, *366*, 112–121. https://doi.org/10.1016/j.epsl.2013.02.005
Ripepe, M., Ciliberto, S., & Schiava, M. D. (2001). Time constraints for modeling source dynamics of volcanic eruptions at Stromboli. *Journal of Geophysical Research*, *106*(B5), 8713–8727. https://doi.org/10.1029/2000jb900374
Ripepe, M., & Gordeev, E. (1999). Gas bubble dynamics model for shallow volcanic tremor at Stromboli. *Journal of Geophysical Research*, *104*(B5), 10639–10654. https://doi.org/10.1029/98jb02734
Roggensack, K., Hervig, R. L., McKnight, S. B., & Williams, S. N. (1997). Explosive basaltic volcanism from Cerro Negro volcano: Influence of volatiles on eruptive style. *Science*, *277*(5332), 1639–1642. https://doi.org/10.1126/science.277.5332.1639

Rose, W. I., Self, S., Murrow, P. J., Bonadonna, C., Durant, A. J., & Ernst, G. G. J. (2008). Nature and significance of small volume fall deposits at composite volcanoes: Insights from the October 14, 1974 Fuego eruption, Guatemala. *Bulletin of Volcanology*, *70*(9), 1043–1067. https://doi.org/10.1007/s00445-007-0187-5

Sable, J. E., Houghton, B. F., del Carlo, P., & Coltelli, M. (2006). Changing conditions of magma ascent and fragmentation during the Etna 122 BC basaltic eruption: Evidence from clast microtextures. *Journal of Volcanology and Geothermal Research*, *158*(3–4), 333–354. https://doi.org/10.1016/j.jvolgeores.2006.07.006

Sable, J. E., Houghton, B. F., Wilson, C. J. N., & Carey, R. J. (2009). Eruption mechanisms during the climax of the Tarawera 1886 basaltic Plinian eruption inferred from microtextural characteristics of the deposits. In T. Thordason, S. Self, G. Larsen, S. K. Rowland, & A. Höskuldsson (Eds.), *Special publications in studies in volcanology: The legacy of George Walker, Spec. Publ. IAVCEI* (Vol. 2, pp. 129–154). Geological Society London. https://doi.org/10.1144/iavcel002.7

Sparks, R. S. J. (1978). The dynamics of bubble formation and growth in magmas: A review and analysis. *Journal of Volcanology and Geothermal Research*, *3*(1–2), 1–37. https://doi.org/10.1016/0377-0273(78)90002-1

Sparks, R. S. J., Barclay, J., Jaupart, C., Mader, H. M., & Phillips, J. C. (1994). Physical aspects on magma degassing, I. Experimental and theoretical constraints on vesiculation. *Reviews in Mineralogy*, *30*, 413–445.

Sparks, R. S. J., Bursik, M. I., Carey, S. N., Gilbert, J. S., Glaze, L. S., Sigurdsson, H., & Woods, A. W. (1997). *Volcanic plumes* (p. 574). Wiley.

Spilliaert, N., Métrich, N., & Allard, P. (2006). S-Cl-F degassing pattern of water-rich alkali basalt: Modelling and relationship with eruption styles on mount Etna volcano. *Earth and Planetary Science Letters*, *248*(3–4), 772–786. https://doi.org/10.1016/j.epsl.2006.06.031

Stelling, P., Beget, J., Nye, C., Gardner, J., Devine, J. D., & George, R. M. M. (2002). Geology and petrology of ejecta from the 1999 eruption of Shishaldin Volcano, Alaska. *Bulletin of Volcanology*, *64*(8), 548–561. https://doi.org/10.1007/s00445-002-0229-y

Szramek, L. A. (2016). Mafic Plinian eruptions: Is fast ascent required? *Journal of Geophysical Research*, *121*, 7119–7136. https://doi.org/10.1002/2016JB013208

Szramek, L., Gardner, J. E., & Hort, M. (2010). Cooling-induced crystallization of microlite crystals in two basaltic pumice clasts. *American Mineralogist*, *95*(4), 103–109. https://doi.org/10.2138/am.2010.3270

Tam, C. K. W. (2019). A phenomenological approach to jet noise: The two-source model. *Philosophical Transactions of the Royal Society A*, *377*(2159), 20190078. https://doi.org/10.1098/rsta.2019.0078

Tam, C. K. W., Viswanathan, K., Ahuja, K. K., & Panda, J. (2008). The sources of jet noise: Experimental evidence. *Journal of Fluid Mechanics*, *615*, 253–292. https://doi.org/10.1017/S0022112008003704

Thompson, G. (2023). A web-based near-real-time seismic monitoring system for Alaskan volcanoes, gthompson/IceWeb2000 [Computer Software]. *IceWeb (Version v1.0.1)*. https://doi.org/10.5281/zenodo.7826053

Thompson, G., McNutt, S. R., & Tytgat, G. (2002). Three distinct regimes of volcanic tremor associated with the eruption of Shishaldin volcano, Alaska, April 1999. *Bulletin of Volcanology*, *64*(8), 535–547. https://doi.org/10.1007/s00445-002-0228-z

Thörarinsson, S., & Sigvaldason, G. E. (1972). The Hekla eruption of 1970. *Bulletin of Volcanology*, *36*(2), 269–288. https://doi.org/10.1007/bf02596870

Toramaru, A. (1995). Numerical study of nucleation and growth of bubbles in viscous magmas. *Journal of Geophysical Research*, *100*(B2), 1913–1931. https://doi.org/10.1029/94jb02775

Toramaru, A. (2006). BND (bubble number density) decompression rate meter for explosive volcanic eruptions. *Journal of Volcanology and Geothermal Research*, *154*(3–4), 303–316. https://doi.org/10.1016/j.jvolgeores.2006.03.027

Valdivia, P., Marshall, A. A., Brand, B. D., Manga, M., & Huber, C. (2022). Mafic explosive volcanism at Llaima volcano: 3D x-ray microtomography reconstruction of pyroclasts to constrain shallow conduit processes. *Bulletin of Volcanology*, *84*(1), 2. https://doi.org/10.1007/s00445-021-01514-8

Vergniolle, S. (1996). Bubble size distribution in magma chambers and dynamics of basaltic eruptions. *Earth and Planetary Science Letters*, *140*(1–4), 269–279. https://doi.org/10.1016/0012-821x(96)00042-8

Vergniolle, S. (1998). Modeling two-phase flow in a volcano. Proceedingds of 13th Australasian Fluid Mechnical Conference, Melbourne, 647–650.

Vergniolle, S. (2008). From sound waves to bubbling within a magma reservoir: Comparison between eruptions at Etna (2001, Italy) and Kīlauea (Hawai'i). *Geological Society, London, Special Publications*, *307*(1), 125–146. https://doi.org/10.1144/SP307.8

Vergniolle, S. (2024a). A web-interface to estimate magma viscosity [dataset], degassing parameters at Shishaldin [software written in Matlab, version 2018b] and foam drainage in laboratory experiments [dataset and software written in Matlab, version 2018b]. *Dataverse (version v1.0.1)*. Retrieved from https://dataverse.ipgp.fr/dataset.xhtml?persistentId=doi:10.18715/IPGP.2023.lj5wjhw6

Vergniolle, S. (2024b). Origin of basaltic Subplinian eruption at Shishaldin volcano (Alaska): A vigorously degassing magma reservoir hosting small bubbles, this issue.

Vergniolle, S., Boichu, M., & Caplan-Auerbach, J. (2004). Acoustic measurements of the 1999 basaltic eruption of Shishaldin volcano, Alaska: 1. Origin of Strombolian activity. *Journal of Volcanology and Geothermal Research*, *137*(1–3), 109–134. https://doi.org/10.1016/j.jvolgeores.2004.05.003

Vergniolle, S., & Bouche, E. (2016). Gas-driven lava lake fluctuations at Erta 'Ale volcano (Ethiopia) revealed by MODIS measurements. *Bulletin of Volcanology*, *78*(60), 1–28. https://doi.org/10.1007/s00445-016-1047-y

Vergniolle, S., & Brandeis, G. (1996). Strombolian explosions: A large bubble breaking at the surface of a lava column as a source of sound. *Journal of Geophysical Research*, *101*(B9), 20433–20448.

Vergniolle, S., & Caplan-Auerbach, J. (2004). Acoustic measurements of the 1999 basaltic eruption of Shishaldin volcano, Alaska: 2. Precursor to the Subplinian activity. *Journal of Volcanology and Geothermal Research*, *137*(1–3), 135–151. https://doi.org/10.1016/s0377-0273(04)00153-2

Vergniolle, S., & Caplan-Auerbach, J. (2006). Basaltic thermals and Subplinian plumes: Constraints from acoustic measurements at Shishaldin volcano, Alaska. *Bulletin of Volcanology*, *68*(7–8), 611–630. https://doi.org/10.1007/s00445-005-0035-4

Vergniolle, S., & Gaudemer, Y. (2012). Decadal evolution of a degassing magma reservoir unravelled from fire fountains produced at Etna between 1989 and 2001. *Bulletin of Volcanology*, *74*(3), 725–742. https://doi.org/10.1007/s00445-011-0563-z

Vergniolle, S., & Gaudemer, Y. (2015). From reservoirs and conduits to surface: Review on the role of bubbles in driving basaltic eruptions, *AGU monography. Hawaiian Volcanism: From Source to Surface*, *208*, 289–322.

Vergniolle, S., & Jaupart, C. (1990). The dynamics of degassing at Kīlauea volcano, Hawai'i. *Journal of Geophysical Research*, *95*(B3), 2793–2809. https://doi.org/10.1029/jb095ib03p02793

Vergniolle, S., & Métrich, N. (2022). An interpretative view of open–vent volcanoes. *Bulletin of Volcanology*, *84*(9), 83. https://doi.org/10.1007/s00445-022-01581-5

Walker, D., & Mullins, O., Jr. (1981). Surface tension of natural silicates from 1200 to 1,500°C and implications for melt structure. *Contributions to Mineralogy and Petrology*, *76*(4), 455–462. https://doi.org/10.1007/bf00371487

Walker, G. P. L., Self, S., & Wilson, L. (1984). Tarawera 1886, New Zealand–a basaltic Plinian fissure eruption. *Journal of Volcanology and Geothermal Research*, *21*(1–2), 61–78. https://doi.org/10.1016/0377-0273(84)90016-7

Wallis, G. B. (1969). *One dimensional two-phase flows* (p. 408). Mc Graw Hill.

Williams, S. N. (1983). Plinian airfall deposits of basaltic composition. *Geology*, *11*(4), 211–214. https://doi.org/10.1130/0091-7613(1983)11<211:padobc>2.0.co;2

Williams, H., & McBirney, A. R. (1979). *Volcanology* (p. 397). Freeman Cooper.

Wong, L. J., & Larsen, J. F. (2010). The Middle Scoria sequence: A Holocene violent strombolian, subplinian and phreatomagmatic eruption of Okmok volcano, Alaska. *Bulletin of Volcanology*, *72*(1), 17–31. https://doi.org/10.1007/s00445-009-0301-y

Woods, A. W., & Koyaguchi, T. (1994). Transitions between explosive and effusive eruptions of silicic magmas. *Nature*, *370*(6491), 641–644. https://doi.org/10.1038/370641a0

Woulff, G., & McGetchin, T. R. (1976). Acoustic noise from volcanoes: Theory and experiments. *Geophysical Journal International*, *45*, 601–616.

Yang, X., Davis, P. M., Delaney, P. T., & Okamura, A. T. (1992). Geodetic analysis of dike intrusion and motion of the magma reservoir beneath the summit of Kīlauea volcano, Hawai'i. *Journal of Geophysical Research*, *97*(B3), 3305–3324. https://doi.org/10.1029/91jb02842

References From the Supporting Information

Aki, K., Fehler, M., & Das, S. (1977). Source mechanism of volcanic tremor: Fluid-driven cracks models and their application to Kīlauea eruption. *Journal of Volcanology and Geothermal Research*, *2*(3), 259–287. https://doi.org/10.1016/0377-0273(77)90003-8

Aki, K., & Koyanagi, R. Y. (1981). Deep volcanic tremor and magma ascent mechanism under Kīlauea, Hawai'i. *Journal of Geophysical Research*, *86*(B8), 7095–7110. https://doi.org/10.1029/jb086ib08p07095

Almendros, J., Chouet, B. A., & Dawson, P. A. (2001). Spatial extent of hydrothermal system at Kīlauea volcano, Hawai'i, determined from array analysis of shallow long-period seismicity, 2: Results. *Journal of Geophysical Research*, *106*(13), 581–13597.

Battaglia, J., & Aki, K. (2003). Location of seismic events and eruptive fissures on the Piton de la Fournaise volcano using seismic amplitudes. *Journal of Geophysical Research*, *108*(B8), 2364. https://doi.org/10.1029/2002JB002193

Battaglia, J., Got, J.-L., & Okubo, P. (2003). Location of long-period events below Kīlauea Volcano using seismic amplitudes and accurate relative relocation. *Journal of Geophysical Research*, *108*(B12), 2553. https://doi.org/10.1029/2003JB002517

Bhakta, A., & Ruckenstein, E. (1997). Decay of standing foams: Drainage, coalescence and collapse. *Advances in Colloid and Interface Science*, *70*, 1–124. https://doi.org/10.1016/s0001-8686(97)00031-6

Chouet, B. (2009). Volcanoes, non-linear processes. In R. Meyers (Ed.), *Encyclopedia of complexity and system science* (Vol. 10, pp. 9782–9899). Springer.

Chouet, B. A., Dawson, P. B., James, M. R., & Lane, S. J. (2010). Seismic source mechanism of degassing bursts at Kīlauea Volcano, Hawai'i: Results from waveform inversion in the 10-50 s band. *Journal of Geophysical Research*, *115*(B9), B09311. https://doi.org/10.1029/2009JB006661

Chouet, B. A., & Matoza, R. S. (2013). A multi-decadal view of seismic methods for detecting precursors of magma movement and eruption. *Journal of Volcanology and Geothermal Research*, *252*, 108–175. https://doi.org/10.1016/j.jvolgeores.2012.11.013

Dehn, J., Dean, K. G., Engle, K., & Izbekov, P. (2002). Thermal precursors in satellite images of the 1999 eruption of Shishaldin Volcano. *Bulletin of Volcanology*, *64*(8), 525–534. https://doi.org/10.1007/s00445-002-0227-0

Delle Donne, D., Aiuppa, A., Bitetto, M., d'Aleo, R., Coltelli, M., Coppola, D., et al. (2019). Changes in SO_2 flux regime at Mt. Etna captured by automatically processed ultraviolet camera data. *Remote Sensing*, *11*(10), 1201. https://doi.org/10.3390/rs11101201

Fehler, M. (1983). Observations of volcanic tremor at Mount St Helens volcano. *Journal of Geophysical Research: Solid Earth*, *88*, 3476–3484.

Haney, M. M., Matoza, R. S., Fee, D., & Aldridge, D. F. (2018). Seismic equivalents of volcanic jet scaling laws and multipoles in acoustics. *Geophysical Journal International*, *213*(1), 623–636. https://doi.org/10.1093/gji/ggx554

Jolly, A. D., Thompson, G., & Norton, G. E. (2002). Locating pyroclastic flows on Soufriere Hills Volcano, Montserrat, West Indies, using amplitude signals from high dynamic range instruments. *Journal of Volcanology and Geothermal Research*, *118*(3–4), 299–317. https://doi.org/10.1016/s0377-0273(02)00299-8

Kondo, G., Aoyama, H., Nishimura, T., Ripepe, M., Lacanna, G., Genco, R., et al. (2019). Gas flux cyclic regime at an open vent magmatic column inferred from seismic and acoustic records. *Nature Scientific Report*, *9*(1), 5678. https://doi.org/10.1038/s41598-019-42033-z

McNutt, S. R. (1994). Volcanic tremor amplitude correlated with eruption explosivity and its potential use in determining ash hazards to aviation, US. *Geological Survey Bulletin*, *2047*, 377–385.

Métaxian, J.-P., Lesage, P., & Dorel, J. (1997). Permanent tremor of Masaya volcano, Nicaragua: Wave field analysis and source location. *Journal of Geophysical Research*, *102*(B10), 22529–22545. https://doi.org/10.1029/97jb01141

Nadeau, P. A., Palma, J. L., & Waite, G. P. (2011). Linking volcanic tremor, degassing, and eruption dynamics via SO_2 imaging. *Geophysical Research Letters*, *38*(1), L01304. https://doi.org/10.1029/2010GL045820

Nadeau, P. A., Werner, C. A., Waite, G. P., Carn, S. A., Brewer, I. D., Elias, T., et al. (2015). Using SO2 camera imagery and seismicity to examine degassing and gas accumulation at Kīlauea Volcano, May 2010. *Journal of Volcanology and Geothermal Research*, *300*, 70–80. https://doi.org/10.1016/j.jvolgeores.2014.12.005

Prejean, P. G., & Brodsky, E. E. (2011). Volcanic plume height measured by seismic waves based on a mechanical model. *Journal of Geophysical Research: Solid Earth*, *116*, B01306. https://doi.org/10.1029/2010JB007620

Rintoul, M. D., & Torquato, S. (1997). Precise determination of the critical thershold and exponents in a three-dimensional continuum percolation model. *Journal of Physics A: Mathematical and General*, *30*(16), L585–L592. https://doi.org/10.1088/0305-4470/30/16/005

Ripepe, M., Poggi, P., Braun, T., & Gordeev, E. (1996). Infrasonic waves and volcanic tremor at Stromboli. *Geophysical Research Letters*, *23*(2), 181–184.

Vicsek, T., & Kertesz, J. (1981). Monte-Carlo renormalisation group approach to percolation on a continuum. *Journal of Physics A*, *14*(L31), L31–L37. https://doi.org/10.1088/0305-4470/14/2/003

Williams-Jones, G., Stix, J., Heiligmann, M., Barquero, J., Fernandez, E., & Gonzalez, E. D. (2001). A model of degassing and seismicity at Arenal Volcano, Costa Rica. *Journal of Volcanology and Geothermal Research*, *108*(1–4), 121–139. https://doi.org/10.1016/s0377-0273(00)00281-x